Andean Geology 53 (2): 336-361. May, 2026
doi: 10.5027/andgeoV53n2-3885

Andean Geology
www.andeangeology.cl

SPECIAL ISSUE: RESEARCH ON THE SOUTH WEST MARGIN OF GONDWANA

Exploring slip partitioning in the Southern Andes: New insights from fault slip data and crustal seismicity

***José Cembrano[1], Alain Lavenu[2], Constanza Rojas[3], Pablo Iturrieta[4], Nicolás Pérez-Estay[5], Ashley Stanton-Yonge[6], Javiera Ruz-Ginouves[7], Pamela Pérez-Flores[8], Gerd Sielfeld[9], Gabriela Zañartu[1], Rebecca Pearce[10], Almudena Sánchez de la Muela[11], Tomás Roquer[12], Isabel Santibáñez[13], Tiaren García[14], Flavia Rojas[15], Pablo Sánchez-Alfaro[16], Simone Masoch[6, 17], Thomas Mitchell[18], Gloria Arancibia[1], Ashley Griffith[19], John Browning[18], Karin Hofer-Apostolidis[20], Gonzalo Yáñez[1]**

[1] *Departamento de Ingeniería Estructural y Geotécnica, Pontificia Universidad Católica de Chile Vicuña Mackenna 4860, Santiago, Chile.*
jcembrano@uc.cl, garancibia@uc.cl, gyaneza@uc.cl, gabrielazanartu@uc.cl

[2] *10 rue de Cedres 64110, Gelos, France.*
alavenu2@orange.fr

[3] *Parcela 3, Camino El Yeco Tunquen, ruta F814, Algarrobo, Chile.*
corojas1@gmail.com

[4] *GFZ Helmholtz Centre for Geosciences, Telegrafenberg 14473 Potsdam, Germany.*
pciturri@gfz.de

[5] *Department of Earth Ocean and Atmospheric Science, University of British Columbia, Vancouver, Canada.*
nnperezestay@eoas.ubc.ca

[6] *Università degli Studi di Padova, Dipartamento di Geoscienze, Via Giovanni Gradenigo, 6, 35131 Padova PD, Italia.*
ashley.sesnic.18@ucl.ac.uk

[7] *Department of Geology, University of Otago, 360 Leith Street, Dunedin, New Zealand.*
javiera.ruz@postgrad.otago.ac.nz

[8] *CIGEA (Consultoría Geológico Ambiental Ltda.), Manuel Rojas 23 Terrazas de Amancay, Huasco, Chile.*
pperezflores@gmail.com

[9] *University of Auckland, Faculty of Science, 23 Symonds Street 1010, Auckland, New Zealand.*
gerd.sielfeld@auckland.ac.nz

[10] *Royal Roads University, Cascade Institute, 2005 Sooke Rd, Victoria, Canada.*
pearce@cascadeinstitute.org

[11] *Consejo Superior de Investigaciones Científicas, Instituto Geológico y Minero de España, Departamento de Riesgos Geológicos y Cambio Climático, Ríos Rosas 23, Madrid, España.*
asmgarzon@ucm.es

[12] *Departamento de Ingeniería de Minas, Metalurgia y Materiales, Universidad Técnica Federico Santa María, Av. Vicuña Mackenna 3939, Santiago, Chile.*
tomas.roquer@usm.cl

[13] *Las Hortensias 2546, Santiago, Chile.*
isantiboric@gmail.com

[14] *SRK Consulting Chile, Hydrogeology Area, Vitacura 2939, 9th floor, Santiago, Chile.*
tiaren.garcia@gmail.com

[15] *University of Manchester, Department of Earth and Environmental Sciences, Oxford Road M13 9PL, Manchester, UK.*
flavia.rojasguzman@manchester.ac.uk

[16] *Universidad Austral de Chile, Facultad de Ciencias, Avenida Rector Eduardo Morales Miranda s/n, Valdivia, Chile.*
pablo.sanchez@uach.cl

[17] *Nevada Seismological Laboratory, University of Nevada, Reno, USA.*
smasoch@unr.edu

[18] *University College London, Department of Earth Sciences, Gower Street, London, UK.*
tom.mitchell@ucl.ac.uk; j.browning@ucl.ac.uk

[19] *School of Earth Sciences, The Ohio State University, 43210, Columbus, Ohio, USA.*
griffith.233@osu.edu

[20] *Swiss Federal Institute of Technology in Lausanne (EPFL), Lausanne, Switzerland.*
karin.hoferapostolidis@epfl.ch

** Corresponding author: jcembrano@uc.cl*

ABSTRACT. Active slip partitioning between the subduction megathrust and the upper plate is investigated in the oblique-convergence setting of the Nazca-South American plate boundary between 33° and 47° S. This segment has two major along-strike bends: the Maipo Orocline (~34° S) and the Arauco Peninsula (~38° S), whereas south of 38° S, lies the intra-arc Liquiñe-Ofqui Fault System (LOFS). Here we examine long- and short-term upper-plate deformation by combining a harmonized catalog of about 2,300 fault-slip measurements in the forearc and arc regions, from which we derive P-T axes using kinematic inversions, along with an integrated seismological database for upper-plate events (1976-2025), including global and local networks. These data are categorized by forearc, arc, and back-arc regions. We identify four distinct tectonic segments based on the spatial distribution of P and T axes in the long-and short-term: (1) 33°-34° S, showing both ~E-W and ~N-S subhorizontal shortening in the forearc and arc areas, suggesting active radial shortening; (2) 34°-37° S, dominated by mostly blind, seismogenic, margin-parallel dextral faults along with NW- and NE-trending structures running at a high angle with respect to the plate margin (called transverse faults here); (3) 37°-41° S, where margin-orthogonal subhorizontal shortening in the submerged forearc coexists with nearly margin-parallel shortening in the emerged forearc, with contemporaneous dextral slip along the LOFS and ~E-W shortening accommodated by transverse NE-trending dextral and NW-trending sinistral seismically active faults; and (4) 41°-47° S, a region governed mainly by the geometry and kinematics of the LOFS strike-slip duplex. Kinematic indicators on mesoscopic faults (mostly slickenfibers) and a lack of pseudotachylytes suggest a considerable aseismic component to upper-plate fault slip, implying that morphotectonic slip rates may overestimate seismic hazard. Future detailed geodetic data may help better constrain the relative contributions of aseismic and seismic slip on the upper-plate faults in this Andean segment.

Keywords: Slip partitioning, Oblique convergence, Andean segmentation, Seismic hazard.

RESUMEN. Explorando la partición del deslizamiento en los Andes del Sur: Nuevas perspectivas a partir de datos de deslizamiento de fallas y sismicidad cortical. La partición del vector de convergencia entre la zona de subducción y la placa superior es analizada en el contexto de la convergencia oblicua entre las placas de Nazca y Sudamérica, desde los 33° S hasta los 47° S. Este segmento presenta dos marcadas curvaturas en el margen continental: el Oroclino de Maipo (~34° S) y la Península de Arauco (~38° S), mientras que al sur de los 38° S se desarrolla, en el dominio de intra-arco, el Sistema de Fallas Liquiñe-Ofqui (SFLO). En este trabajo se examina la deformación de la placa superior mediante un catálogo de aproximadamente 2.300 mediciones de fallas en las regiones del antearco y del arco, junto con datos sismológicos de eventos entre 1976 y 2025, procedentes de redes globales y locales, categorizados como de antearco, arco y trasarco. Se identifican cuatro segmentos tectónicos con base en la distribución espacial de los ejes P y T: (1) 33°-34° S, con acortamiento subhorizontal en direcciones ~E-O y ~N-S, lo que sugiere acortamiento radial; (2) 34°-37° S, dominado por fallas dextrales, en su mayoría ciegas, sismogénicas y paralelas a la margen, junto con estructuras sismogénicas de rumbo NO y NE; (3) 37°-41° S, donde coexiste un acortamiento ortogonal al margen en el antearco sumergido con otro paralelo al margen en el antearco emergido. Adicionalmente, ocurren fallas transversales sísmicamente activas, NO y NE, sinistrales y dextrales, respectivamente; y (4) 41°-47°, una región gobernada principalmente por la geometría y cinemática del SFLO. Indicadores cinemáticos en fallas mesoscópicas (*e.g.,* fibras de crecimiento) y la ausencia de pseudotaquilitas sugieren una componente asísmica significativa, lo que puede llevar a sobreestimar el peligro sísmico calculado mediante estimaciones morfotectónicas. Futura información geodésica de detalle puede contribuir a discriminar de mejor manera el deslizamiento sísmico del asísmico en las fallas de la placa superior de este segmento de los Andes.

Palabras clave: Partición del deslizamiento, Convergencia oblicua, Segmentacion andina, Peligro sísmico.

1. Introducción

The partitioning of upper plate deformation at obliquely convergent margins has been studied for over fifty years (*e.g.,* Fitch, 1972; Jarrard, 1986; Beck, 1991; McCaffrey, 1992, 1996; Canora *et al.,* 2014; Stanton-Yonge *et al.,* 2016). Early research by Fitch (1972) proposed that the oblique convergence vector is partitioned into margin-orthogonal and margin-parallel slip components, with the former mainly accommodated by the subduction zone and the latter by an intra-arc strike-slip fault system within the upper plate. Beck (1991) and McCaffrey (1992) provided important insights by suggesting that most obliquely convergent margins only show partial slip partitioning, where only part of the oblique convergence is absorbed by oblique displacement at the plate boundary, leading to a smaller residual margin-parallel slip vector than otherwise assumed in earlier studies. Some years later, De Saint Blanquat *et al.* (1998) refined earlier deformation and slip partitioning models by proposing a conceptual framework for

transpressional magmatic arcs as a general model for obliquely convergent margins (Teyssier *et al.,* 1995). In their model, they define margin-parallel domains in the upper plate that accommodate not only one component of the convergence vector but different degrees and combinations of strike-slip and shortening deformation (Fig. 1). This framework was further improved and applied to the specific case of the Southern Andes by Lavenu and Cembrano (1999).

Recent seismological studies in the Chilean margin have suggested that the accommodation of the margin-parallel component of the plate convergence vector within the upper plate is more complex than previously understood (*e.g.,* Sielfeld *et al.,* 2019a; Pérez-Estay *et al.,* 2020). These studies revealed significant variations in earthquake focal mechanisms within the brittle crust of the continental plate, in both kinematics and orientations. Structural geology studies have independently reported similar behavior in the long-term deformation recorded in exhumed faults, suggesting that the margin-parallel component is accommodated by numerous reactivated and new faults with varying strike, dip, and kinematics, many of which show evidence of activity from the Pliocene to the Quaternary (Pérez-Flores *et al.,* 2016; Sielfeld *et al.,* 2017). Numerical models support these field observations, highlighting the importance of fault strike relative to the margin and showing that a range of fault kinematics can coexist to accommodate the margin-parallel slip component (Stanton-Yonge *et al.,* 2016). Analog models of the Southern Andean oblique subduction plate margin are consistent with these observations as well (*e.g.,* Eisermann *et al.,* 2021).

Overall, evidence from seismology, structural geology, and numerical modeling suggests that slip complexity involves not only margin-parallel faults but also transverse faults, which significantly contribute to accommodating fault slip in the upper plate. In this study, we present a review of the existing published seismological and field structural data for the Southern Andes between 33° and 47° S, a segment marked by the end of flat subduction in the north (*e.g.,* Jordan *et al.,* 1983) and the Chile Triple Junction in the south (*e.g.,* Forsythe and Nelson, 1985). This continental segment features two sharp inflections of the plate margin, one at ~34° S (Maipo Orocline) and another around 38° S (Arauco Peninsula) (Fig. 2). Notably, two significant earthquake rupture zones associated with subduction megathrust earthquakes overlap at the Arauco Peninsula: the 2010 Maule earthquake and the 1960 Valdivia earthquake (*e.g.,* Moreno *et al.,* 2009, 2012; Vigny *et al.,* 2011). This latter region therefore represents a critical tectonic element of the plate margin (*e.g.,* Melnick *et al.,* 2009), marking a slight but significant change in plate obliquity (*e.g.,* Stanton-Yonge *et al.,* 2016) (Fig. 2).

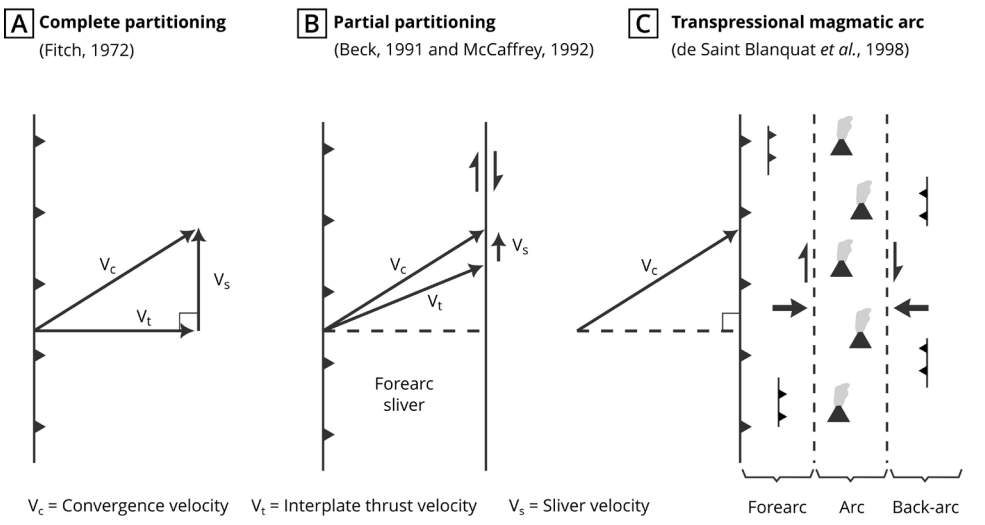

FIG. 1. Schematic diagram illustrating the evolution of the slip partitioning concept over the past five decades. **A.** Complete partitioning of the convergence slip vector (Fitch, 1972). **B.** Partial partitioning (*e.g.*, Beck, 1991; McCaffrey, 1992). **C.** Slip partitioning considering a transpressional magmatic arc domain (De Saint Blanquat *et al.*, 1998).

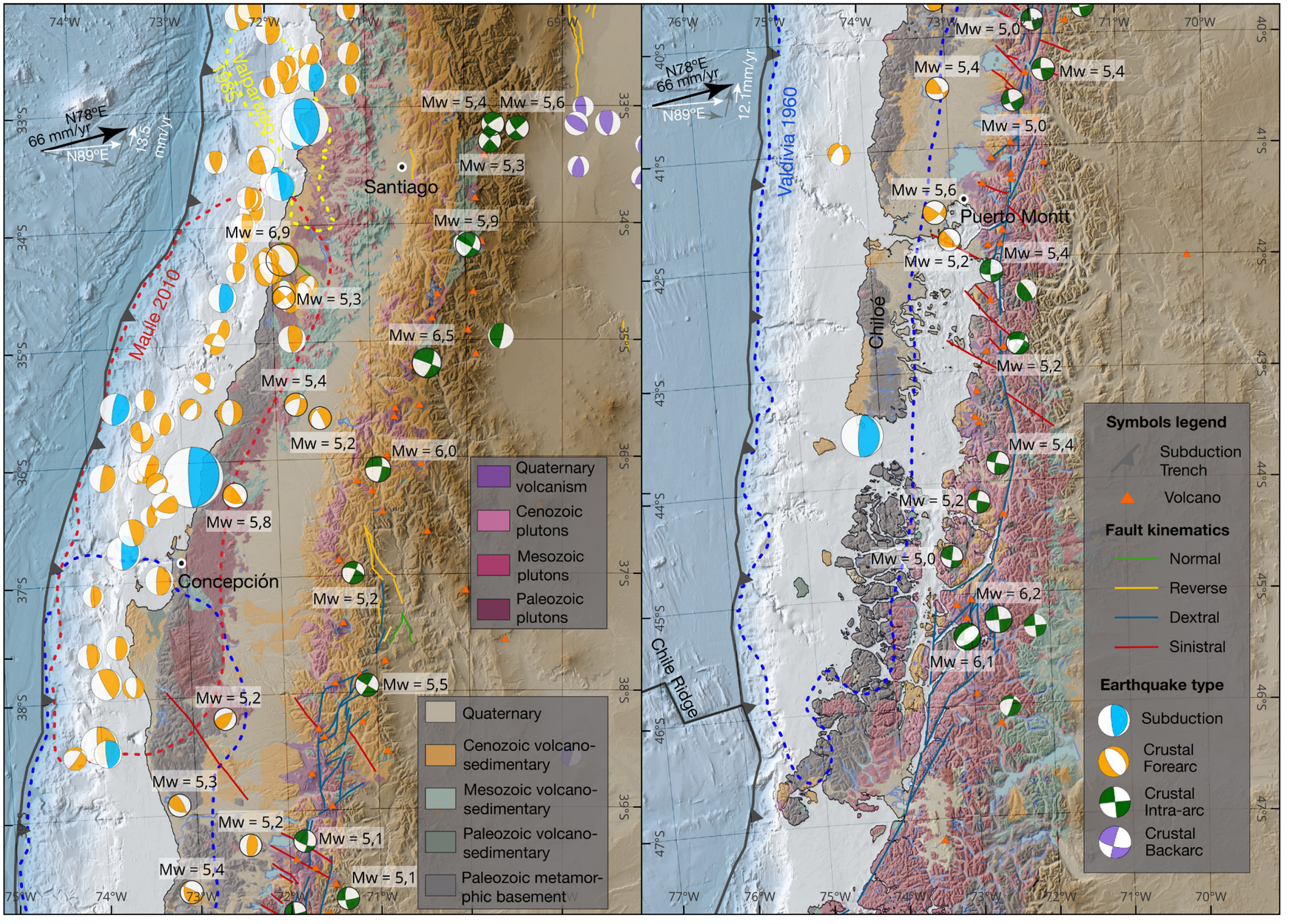

FIG. 2. Tectonic, geological, and seismological setting of the Chilean Andes between 33° and 47° S, mainly based on Sernageomin (2003), Cembrano and Lara (2009), Tapia *et al.* (2015), Stanton-Yonge *et al.* (2016), Sielfeld *et al.* (2019a), and Olivar *et al.* (2022). Main Quaternary crustal faults (data from Santibáñez *et al.*, 2019 and Costa *et al.*, 2020), and Holocene volcanoes are included for reference. Crustal seismicity in the overriding plate is shown for earthquakes with Mw>5.0 based on data from global networks. Selection subduction interface events (Stanton-Yonge *et al.*, 2016) are displayed alongside crustal seismicity. The segmented blue line indicates the rupture zone of the Mw 9.5 1960 Valdivia earthquake (Moreno *et al.*, 2009), the red segmented line marks the Mw 8.8 2010 Maule earthquake (Moreno *et al.*, 2012), and the yellow segmented line shows the Mw 8.0 1985 Valparaíso earthquake (Bravo *et al.*, 2019). The partitioning of the convergence vector (N78°E, black arrow) into its margin-parallel and margin-orthogonal (grey arrows) components is depicted for the regions between 34° and 38° S (where the margin trends N20°E), and between 38° and 47° S (where the margin trends N10°E). The average slip vector of subduction earthquakes (N89°E; Stanton-Yonge *et al.*, 2016) is also shown (white arrow in between the convergence vector and the orthogonal to the trench), illustrating the partial partitioning of convergence along the margin. The residual margin-parallel component to be accommodated within the overriding plate is indicated for both regions (white arrows parallel to the plate margin; 13.5 mm/year for 34°-38° S and 12.1 mm/year for 38°-47° S). The full classified catalog and the P- and T-axes for each earthquake class are shown respectively in figures S1 and S2 in the Supplementary Material. See the Data and Resources chapter for more information on data source compilation and processing.

In this manuscript, we aim to improve our understanding of how deformation and slip resulting from oblique plate convergence are accommodated in the upper plate. Our newly integrated structural and seismological evidence strongly suggests the existence of four consecutive Andean segments that have experienced unique tectonic evolution since the Neogene. This segmentation offers important insights into the fundamental mechanisms underlying plate margin deformation and the seismic hazards (and possible risks) associated with potentially seismogenic faults.

2. Tectonic and geological setting

2.1. Geology and crustal structure of the Southern Andes

The Andean mountain range between 33° and 47° S shows a slightly deformed, rigid, and cold forearc region adjacent to a weaker and hotter magmatic arc domain (*e.g.,* Tassara and Yáñez, 2003; Farías *et al.,* 2006; Cembrano and Lara, 2009; Gerbault *et al.,* 2009). This segment is characterized by a slightly dextral-oblique convergence between the Nazca and South American plates, occurring at a rate of approximately 7 cm/year (*e.g.,* Angermann *et al.,* 1999; Quiero *et al.,* 2022). Oblique convergence has been dominant at the plate margin for the past ~20 Myr (Pardo-Casas and Molnar, 1987; Somoza, 1998), with slight transient variations in the obliquity angle (<10°) on timescales of a few Myr (Quiero *et al.,* 2022). The southern boundary of the study region is defined by the Chile Triple Junction, where the active Chile Ridge, which separates the Nazca plate from the Antarctic plate, is subducted beneath the continent (Figs. 2 and 3).

The regional geological units between 33° and 47° S form belts roughly parallel to the margin, from Paleozoic plutonic, volcano-sedimentary, and metamorphic rocks in the forearc to Meso-Cenozoic plutonic and volcano-sedimentary formations in the arc and back-arc regions (Fig. 2). In between, scattered outcrops of Oligocene-Miocene rocks, predominantly obscured by more recent volcano-sedimentary deposits, are present (Fig. 2).

Between 33° and 38° S, the basement rock units of the volcanic arc consist primarily of extensive outcrops of Meso-Cenozoic volcanic and volcano-sedimentary rocks, locally intruded by Neogene plutons (*e.g.,* Charrier *et al.,* 2002; Farías, *et al.,* 2007; Piquer *et al.,* 2010; Pearce *et al.,* 2020) (Fig. 2). This setting dramatically changes south of ~38° S, where volcanoes are mostly constructed directly on top of Meso-Cenozoic plutonic rocks (Hervé, 1994; Stern *et al.,* 2011) (Fig. 2). Consistently, Cenozoic regional exhumation rates, determined using both apatite and zircon fission track data along the main range, show a sharp increase at around 38° S. There, exhumation rates jump from <0.1 mm/year in the north to >1 mm/year to the south (*e.g.,* Thompson, 2002; Glodny *et al.,* 2008).

Moreover, the crustal thickness beneath the magmatic arc steadily decreases from approximately 55 km at 33° S to 35 km at 46° S, paralleled by a decline in the average elevation of the Main Cordillera, from 5,000 m to under 2,000 m (Tassara and Yáñez, 2003; Cembrano and Lara, 2009).

2.2. Short-term slip partitioning

To characterize the short-term crustal deformation between 33° and 47° S, we compiled a comprehensive focal-mechanism catalog of Mw>5.0 earthquakes in the upper plate, spanning the entire forearc, arc and back-arc regions (Fig. 2). Compiled from global network sources, the catalog aims to provide a present-day snapshot of the state of stress and slip partitioning along and across the plate boundary. Relevant (Mw>7.0) subduction earthquakes were also recorded (Stanton-Yonge *et al.,* 2016), enabling the calculation of the margin-parallel component of oblique subduction and its variation along strike (Fig. 2).

The dataset was constructed by integrating focal-mechanism solutions from the Global Centroid Moment Tensor (GCMT; Ekström *et al.,* 2012) and the Advanced National Seismic System Comprehensive Catalog (ANSS-ComCat; USGS, 2017), harmonizing them into a unified format and retaining events within the study area from 1976 to 2025. Events were filtered, merged, and checked for duplicates (*e.g.,* Weatherill *et al.,* 2016), and supplemented with relocated hypocenters where available (Potin *et al.,* 2025). Using slab interface geometry (Hayes *et al.,* 2018) and kinematic criteria similar to those applied in the New Zealand Seismic Hazard Model (*e.g.,* Gerstenberger *et al.,* 2024), we classified events into forearc, intra-arc, and back-arc domains. The classification criteria and the full catalog, further divided into intra-slab, outer-rise, and deep earthquakes, are detailed in figure S1 of the Supplementary Material. The P- and T-axes of earthquakes for each class are

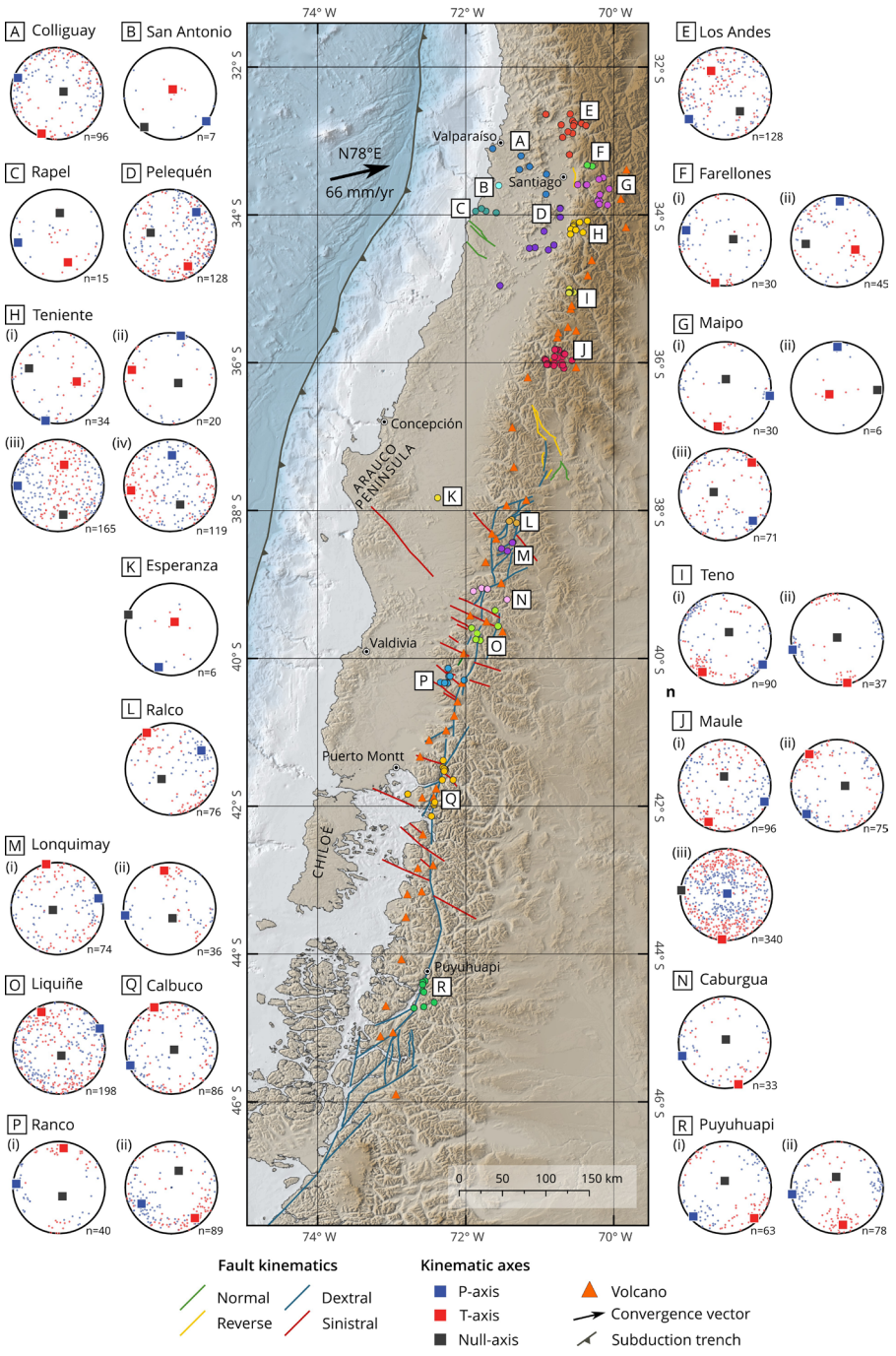

FIG. 3. Compilation and analysis of both published (*e.g.*, Arancibia *et al.*, 1999; Lavenu and Cembrano,1999; Pérez-Flores *et al.*, 2016; Roquer *et al.*, 2022) and new (this study) fault slip data. Structural sites, or combinations of them, are grouped in clusters in case of consistent P-T results (labelled A to R). On the map, each structural site is shown as a circle, colored by cluster group. Clusters with more than one distinct solution are displayed with multiple lower-hemisphere equal-area stereonets, labeled i to iv, depending on the number of additional solutions. All clusters show both the distribution of P and T instantaneous strain axis orientations for all individual faults (blue and red dots), as well as the kinematic axes for the fault population, calculated using the methods established after Marret and Allmendinger (1990) and Allmendinger *et al.* (2012). The maximum shortening axis (P), minimum shortening axis (T), and the null axis are represented as blue, red, and black squares, respectively. Red triangles represent active volcanoes.

shown in figure S2 of the Supplementary Material. More information regarding data processing and accessibility is provided in the Data and Resources chapter at the end of this manuscript.

The seismicity related to the subduction interface exhibits reverse-slip and involves ~N-S striking nodal planes with P-axes trending nearly E-W (Fig. 2). This indicates a P-axis direction slightly rotated clockwise (~10-20°) from the plate margin slip vector (Stanton-Yonge *et al.,* 2016).

In the submerged forearc (west of the coastline), the seismicity is focused in the rupture zones of the Mw 8.8 2010 Maule and Mw 8.0 1985 Valparaíso earthquakes (Fig. 2). Most of these events (41 out of 49; ~84%) are aftershocks of the 2010 megathrust earthquake, and can be grouped into three populations: (1) 37 reverse-slip events with nodal planes striking near N-S and P-axes trending close to E-W, similar to the subduction-related events; (2) nine normal-slip events with nodal planes striking NW, NS, and NE; and (3) three strike-slip events with margin-oblique nodal planes and P-axes trending NE (Fig. 2).

In the emerged forearc (east of the coastline), 23 earthquakes (12 of which occurred before the 2010 Maule earthquake) can be grouped as follows: (1) 11 with margin-oblique nodal planes along the entire margin, either with strike-slip (three), reverse/strike-slip (six), or normal/strike-slip (two) kinematics, exhibiting margin-subparallel P-axes trending from N-S to NE; (2) six normal-slip earthquakes with nodal planes striking near NW and near N-S, five of which are associated with the Mw 6.9 2010 Pichilemu aftershock sequence (*e.g.,* Aron *et al.,* 2013); and (3) six reverse-slip events with nodal planes striking mainly N-S (Fig. 2).

Intra-arc seismicity (28 events) is primarily represented by strike-slip events (Fig. 2), with two exceptions: the normal, dip-slip, Mw 6.1 2007 Aysén earthquake, located at 45.4° S (Legrand *et al.,* 2011), and three reverse-slip earthquakes at 34°, 35°, and 42° S. In the northern part of the study region, between 33° and 34° S, strike-slip events have a nearly E-W oriented horizontal P-axis, with NW- and NE-striking nodal planes, exhibiting sinistral or dextral kinematics, respectively. Between 34° and 37° S, earthquakes show strike-slip kinematics with subvertical nodal planes striking approximately N25°E (dextral) and N65°W (sinistral). South of 37° S, the events show strike-slip kinematics, with nodal planes striking between N20°W and N30°E, mostly oriented from N-S to N10°E. Earthquake kinematics within the southern part of the arc maintain a consistent orientation, characterized by a subhorizontal, NE-trending P-axes, as also documented by local seismological networks (Lange *et al.,* 2008; Pérez-Estay *et al.,* 2020).

2.3. Long-term slip partitioning

The long-term regional-scale structure of the intra-arc and back-arc domains between 33° and 35° S is defined by east-verging, margin-parallel folds and thrusts of Cenozoic age, representing the westernmost part of the Aconcagua and Malargüe foreland fold-and-thrust belts (*e.g.,* Giambiagi and Ramos, 2002). Major regional reverse faults affect the Meso-Cenozoic volcano-sedimentary units, accommodating a limited degree of shortening compared to the Andes of northern Chile (Giambiagi *et al.,* 2012). A similar intra-arc compression regime has been seismically recorded in the 33°-34° S latitude range (Ammirati *et al.,* 2022).

Available fault-slip data document the long-term stress and strain state of the forearc and intra-arc regions since the Pliocene, revealing a local margin-parallel shortening in the forearc and a NE-trending, subhorizontal maximum compression axis (σ_1) across the volcanic arc, the latter prevalent from 37° to 46° S (*e.g.,* Arancibia *et al.,* 1999; Lavenu and Cembrano, 1999; Cembrano *et al.,* 2000; Lara *et al.,* 2006). In the arc domain, the main compressional stress axis aligns with many volcanic features and dike trends (Cembrano and Lara, 2009; Sielfeld *et al.,* 2017), a pattern that is also consistent with contemporaneous margin-parallel dextral strike-slip deformation.

Although margin-parallel reverse faults dominate, there is evidence of conjugate NE-striking dextral and NW-striking sinistral strike-slip faults in the forearc (Aron *et al.,* 2013; Santibáñez *et al.,* 2019), the magmatic arc (*e.g.,* Rivera and Cembrano, 2000; Piquer *et al.,* 2015, 2021), and the foreland (Mescua *et al.,* 2019; Olivar *et al.,* 2022). The major earthquakes recorded between 34-37° S (Mw>6), namely the Mw 6.5 2004 Teno and the Mw 6.0 2012 El Melado, have strike-slip focal mechanisms, confirming the seismogenic nature of the NE- and NW-trending faults in this area (*e.g.,* Sielfeld *et al.,* 2019b). Moreover, these arc-oblique fault systems have been proposed as structural controls on magmatism and mineralization (*e.g.,* Piquer *et al.,* 2015).

Between 36° and 38° S, the Argentine foreland is characterized by the Neogene Chos-Malal and El Agrio fold-and-thrust belts (*e.g.,* Folguera *et al.,* 2004, 2007), with active back-arc volcanism coeval with E-W compression along the El Agrio belt (*e.g.,* Galland *et al.,* 2007). In contrast, the arc region, which lies within a fairly similar latitude range, has undergone arc-orthogonal extension during the Quaternary, accompanied by a minor component of dextral strike-slip displacement (Melnick *et al.,* 2006).

West of the El Agrio lies the Antiñir-Copahue fault zone, an east-vergent, high-angle fault system characterized by dextral transpressive and dextral transtensive faults, which forms the orogenic front at these latitudes (Folguera *et al.,* 2004). This fault zone merges southwestwards with the 1200 km-long Liquiñe-Ofqui Fault System (LOFS), a major intra-arc fault system that extends from 38° to 47° S (Hervé, M., 1976; Hervé *et al.,* 1979; Hervé, 1994; Cembrano *et al.,* 1996; Folguera *et al.,* 2002; Rosenau *et al.,* 2006; Pérez-Flores *et al.,* 2016; Sielfeld *et al.,* 2019a). Evidence from ductile-to-brittle shear zones suggests that the LOFS has been active as a transpressional dextral strike-slip structure for at least the past 6 Myr (Arancibia *et al.,* 1999; Cembrano *et al.,* 2002), and that it may have acted as a leaky transform fault ~25 Ma ago (Hervé *et al.,* 1995). This fault was believed to be spatially and genetically linked to sedimentation, local magma ascent, and concomitant pillow lava formation under a deep-rooted transtensional regime (Hervé *et al.,* 1995). The shortening component of Pliocene-to-recent intra-arc deformation increases to the south as the LOFS approaches the Chile Triple Junction (*e.g.,* Lavenu and Cembrano, 1999; Cembrano *et al.,* 2002; Thompson, 2002; Rosenau *et al.,* 2006).

In the study area, a landmark paper providing an overview of different stress states associated with individual volcanoes is that of Pérez-Estay *et al.* (2023). The study used available fault-slip data and earthquake focal mechanisms to classify volcanoes by their stress states. A key conclusion is that the stress regime along the arc is neither uniform nor of a single type; instead, it exhibits a spatial and/or temporal coexistence of distinct and even opposing stress regimes, a pattern also recognized in previous studies, albeit at more local scales (*e.g.* Pérez-Flores *et al.,* 2016). The most frequently observed regime corresponds to the one initially identified at the regional scale: a strike-slip regime with σ_1 and σ_3 oriented NE and NW, respectively. Additionally, a localized stress regime with a vertical σ_1 has been systematically observed in several large volcanoes, likely resulting from stress rotation driven by magma pressure (Pérez-Estay *et al.,* 2023).

3. Methods and results

3.1. Long-term deformation: fault slip data from crustal faults, a harmonized new compilation.

Over the past 15 years, the quantity and quality of fault-slip data collected in the field, particularly in the volcanic arc region, have significantly improved, yielding new insights into Pliocene and younger slip partitioning and the regional and local strain/stress states (Sánchez *et al.,* 2013; Pérez-Flores *et al.,* 2016; Sielfeld *et al.,* 2019a, b; Ruz-Ginouves *et al.,* 2020; Mura *et al.,* 2025). Figure 3 presents a summary of all the data collected from structural sites mapped by our research group since the early 1990s (see the Data and Resources chapter at the end of this manuscript for the complete dataset). We deliberately included only results from our group because the conceptual approach and field methodology have been applied consistently, using the same geological and structural criteria to define the geometry and kinematics of mesoscopic faults (see, for instance, Pérez-Flores *et al.,* 2016). In the Discussion section these results are placed into a broader literature context.

Our compilation includes around 2,300 mesoscopic fault surfaces, for which we recorded the strike, dip, and rake of the striae. These faults affect Cretaceous to recent rock units, although only those that are clearly post-Miocene were considered in the analysis of current slip partitioning because the plate convergence vector, as stated earlier, has remained nearly constant in magnitude and direction over the past 20 Myr. Faults affecting Cretaceous and Paleogene rock units in the forearc are presented to account for earlier deformation patterns expected to differ from those of neotectonic activity.

Faults were identified and measured along the master and subsidiary faults of the LOFS, along NW- and NE-striking transverse faults in the intra-arc, and at five sites in the forearc (Fig. 3). Fault displacement sense was determined by examining key features on the fault planes, including secondary fractures, mineral crystallization, and tension cracks, among other kinematic indicators (*e.g.,* Petit, 1987).

The orientations of the maximum shortening (P) and maximum stretching (T) instantaneous axes for each fault plane were obtained through FaultKin v.7.4.1 (Marrett and Allmendinger, 1990; Allmendinger *et al.,* 2012), based on the fault plane's orientation and the resolved displacement vector (slickenline). The representative orientations of the P and T axes for a fault population were calculated under the assumption of small single displacements and a consistent deformation field, by assuming a statistical Bingham distribution. Non-clustered P- and/or T-axes suggest kinematic heterogeneity in faulting, which may be caused by factors such as triaxial deformation or reactivation of anisotropies. Neighboring sites with consistent P-T results were grouped to make the data easier to understand and visualize, obtaining 18 clusters (Fig. 3). In eight of these (Farellones, Maipo, Teniente, Teno, Maule, Lonquimay, Ranco, and Puyuhuapi), more than one solution was identified, resulting in two to four P-T axis stereoplots (Fig. 3). As we focus on deformation and slip partitioning rather than stress fields, we chose to present the data in a manner that reflects observations with minimal interpretation, consciously avoiding stress inversion programs. For the interested reader, stress field analyses conducted for the study area can be found in Arancibia *et al.* (1999), Cembrano and Lara (2009), Pérez-Flores *et al.* (2016), Sielfeld *et al.* (2019b), and Pérez-Estay *et al.* (2023), among others.

Overall, regional-scale analysis of the P-T axes from fault slip data in the volcanic arc indicates two primary maximum shortening axes: one oriented N60°E and the other trending ~E-W. In both cases, the minimum shortening axis is predominantly horizontal. When analyzed in greater detail, the following is recognized (Fig. 3):

1. Sites in the forearc between 33° and 34° S were mapped in Cretaceous rock units (Colliguay), while those in Rapel and San Antonio affect Neogene sedimentary rocks. Although these sites exhibit a high dispersion in kinematic axis solutions, both P and T axes are predominantly subhorizontal, with roughly E-W shortening in clusters Colliguay and Rapel. North of 34° S, sites, Farellones and Maipo display a margin-parallel shortening. Sites at Farellones cut Miocene rock units, whereas those at Maipo affect Quaternary strata (Lavenu and Cembrano, 2008). Clusters Pelequén and Los Andes show a higher dispersion in the kinematic axis solutions, but a general NE-trending horizontal P-axis and a NW-trending subhorizontal T-axis. Faults at these sites affect Cretaceous to Miocene rock units.
2. In the volcanic arc north of 34.5° S, a subhorizontal, roughly E-W shortening is also present, as documented at sites Farellones and Maipo. At these sites, extension axes are predominantly subhorizontal to horizontal, whereas at Teniente, just west of the volcanic arc, horizontal N-S shortening is documented. Faults at Teniente cut Pliocene rock units.
3. Farther south, in the Main Cordillera at the Teno site (~35° S), the P-axis solution remains ~E-W, with both P and T subhorizontal. This solution is compatible with the dominant NE-dextral and NW-sinistral strike-slip faults observed in the field. Most of these faults are no older than Oligocene or Miocene.
4. At around 36° S, sites within the intra-arc area (Maule site) were mainly mapped in Oligocene to Pleistocene volcano-sedimentary rocks. Fault-slip analysis reveals three distinct orientations of the P-T axis. The first features a horizontal NE-trending P-axis that aligns with the regional ~N60°E maximum shortening direction. The second displays a horizontal P-axis rotated to N60°W. However, the most prevalent orientation is characterized by a nearly vertical P-axis and a N-S trending T-axis, compatible with E-W striking Pliocene-Pleistocene normal faults.
5. In the forearc at 38° S (Esperanza site), faults that displace Quaternary sedimentary rocks (Lavenu and Cembrano, 1999) show a horizontal N-S trending P-axis with a near-vertical T-axis.
6. Between 38° and 42° S, all clusters within the intra-arc domain exhibit a horizontal to slightly plunging NE-trending P-axis and a horizontal to slightly inclined NW to NNW-trending T-axis. Some individual sites at Lonquimay and Ralco show a slight clockwise rotation of both P- and T-axes towards E-W and N-S trends, respectively. The maximum age of the mapped faults is Miocene.
7. Near the southern end of the study area (~44.5° S), the Puyuhuapi cluster represents faults affecting Miocene and Pliocene rock units. Fault-slip analysis indicates two main kinematic axis solutions: one with a horizontal-to-subhorizontal NE-trending P-axis and a horizontal-to-subhorizontal NW-trending T-axis, and another showing clockwise rotation of both P- and T-axes toward E-W and N-S, respectively.

3.2. Short-term deformation: integrated seismological data from crustal earthquakes from local networks

The availability of seismological data from crustal faults in the southern Andes has significantly increased both in quantity and quality over the past two decades (*e.g.,* Lange *et al.,* 2008; Mora *et al.,* 2010; Legrand *et al.,* 2011; Agurto *et al.,* 2012; Sielfeld *et al.,* 2019a). This has been possible thanks to the deployment of local networks focused on current deformation processes and stress state, particularly for the arc and forearc regions (*e.g.,* Farías *et al.,* 2011; Ammirati *et al.,* 2019; Pearce *et al.,* 2020; Pérez-Estay *et al.,* 2020; Stanton-Yonge *et al.,* 2025). These developments have also enabled the identification of seismogenic faults within known regional-scale fault systems and the potential discovery of unknown concealed faults. Previously, seismic data were mostly accessible only through the U.S. Geological Survey global seismological network, with a few exceptions noted in local studies (Barrientos and Acevedo-Aránguiz, 1992).

We compiled focal mechanisms of seismic activity detected by temporary local networks in and next to the volcanic arc domain (Fig. 4), reported on previously published studies (Lange *et al.,* 2008; Mora *et al.,* 2010; Agurto-Detzel *et al.,* 2014; Ammirati *et al.,* 2019; Sielfeld *et al.,* 2019a; Pérez-Estay *et al.,* 2020; Montenegro *et al.,* 2021; Mura *et al.,* 2025; Stanton-Yonge *et al.,* 2025) to examine the current deformation processes occurring in the overriding plate. Due to variability in magnitudes, azimuthal gaps, and the number of observations at each source, all mechanisms were included, as each dataset comes from a previously validated and published study.

Figure 4d displays the distribution of P-T axes of focal mechanisms identified, along with the number of mechanisms per network. We selected three regions covered by one or more local networks to examine the spatial distribution of microseismicity and crustal faults: Maipo (Ammirati *et al.,* 2019; Fig. 4A), Araucanía (Sielfeld *et al.,* 2019; Montenegro *et al.,* 2021) (Fig. 4B), and Aysén (Mora *et al.,* 2010; Agurto-Detzel *et al.,* 2014; Pérez-Estay *et al.,* 2020) (Fig. 4C). The seismicity detected by the local networks is shown as green dots and ranked by depth, along with a representative subset of focal mechanisms from each network (full focal mechanisms database available in the original references or in the Data and Resources chapter). A detailed discussion about seismicity rates in each region is beyond the scope of this work. Instead, the figures highlight the overall deformation pattern of the upper plate, as reflected in the orientations and distributions of the P and T axes.

The reported seismicity generally covers relatively short time windows (typically between 1 and 3 years of observation) and includes only events with Mw<5.0. Thus, it provides only a partial view of the ongoing processes and does not necessarily represent the activity of major faults. Nevertheless, this information is valuable because: (1) it allows spatial comparison between mapped faults and small earthquakes, and (2) the high density of local stations makes it possible to estimate focal mechanisms of small events that are not included in global catalogs. As our results focus on seismic network deployments within and around the volcanic arc domain, there is an inherent bias toward detecting higher seismicity rates in the arc than in the forearc. However, the global compilation presented in figure 2 partly compensates for this gap.

In figure 4, the current kinematics in the forearc and arc regions are evidenced by numerous shallow crustal earthquakes of relatively small magnitude. The orientations of P-T axes from focal mechanisms indicate a variety of fault kinematics. The main observations are:

Strike-slip focal mechanism solutions primarily characterize the arc region between 34° and 47° S, with isolated normal events and even fewer reverse events (*e.g.,* Chinn and Isacks, 1983; Lange *et al.,* 2008; Sielfeld *et al.,* 2019a; Pérez-Estay *et al.,* 2020). This aligns with the global catalog results shown earlier (Fig. 2). Conversely, the coexistence of reverse and strike-slip focal mechanisms has been recorded only within the Main Cordillera between 33° and 34° S (*e.g.,* Farías *et al.,* 2006; Ammirati *et al.,* 2019) (Fig. 4A). This transition from radial shortening observed north of 34° S (non-partitioned) to partitioned deformation south of 34° S, coincides with a marked increase in convergence obliquity south of 34° S, related to a significant change in trench orientation from nearly N-S to NNE.

In the Maipo area (Fig. 4A), the P-T axes exhibit high dispersion, likely related to local stress perturbations around faults, but reverse kinematics predominate. The nodal plane covers a wide range of orientations, but nearly N-S and E-W trending P-axis solutions are prevalent. Strike-slip kinematics are consistent with predominant E-W shortening.

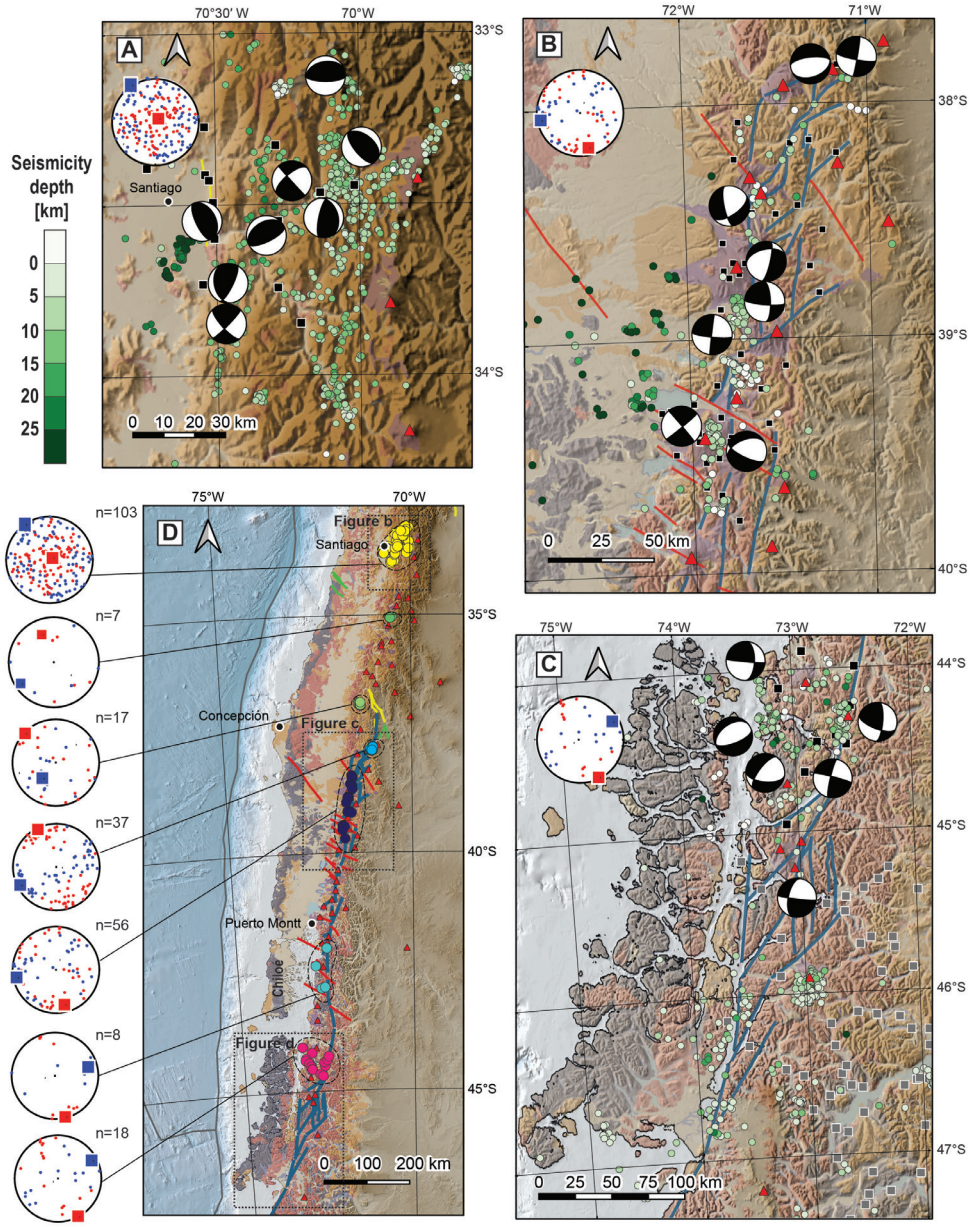

FIG. 4. Compilation and analysis of published crustal seismicity and a subset of focal mechanisms from local seismic networks, including events with Mw<5.0. Black and gray squares mark seismic stations from temporary local network deployments in previous studies, from which the data were compiled. Panels (A), (B), and (C) show insets with previously published seismicity for the Maipo, Araucanía, and Aysén regions, respectively. The Maipo region includes seismicity and focal mechanisms from Ammirati *et al.* (2019). The Araucanía region exhibits seismicity reported by Sielfeld *et al.* (2019a), along with focal mechanisms from the same authors and from Montenegro *et al.* (2021). The Aysén region shows seismicity reported by Agurto-Detzel *et al.* (2014) and Pérez-Estay *et al.* (2020), accompanied by focal mechanisms from Mora *et al.* (2010) and Pérez-Estay *et al.* (2020), the latter referring to the initial state of the 2007 Aysén crisis. Panel (D) shows a regional map with the locations of individual seismic events (colored circles) for which focal mechanism solutions were obtained from different local seismic networks. Each local network is represented by a distinct color. Background geology and structures are as shown in figure 2. The stereonet plots summarize the P- and T-axis orientations of all mechanisms recovered by each local network, with blue and red squares indicating the average P- and T-axis directions for each network, respectively. For more information, the reader is referred to the literature cited in this study and to the Data and Resources chapter.

Farther south, in the Araucanía and Aysén regions (Fig. 4B, C), margin-parallel, strike-slip kinematics predominate, with NE-trending shortening consistent with either dextral slip in subvertical N-to-NNE striking faults, or sinistral slip in WNW-striking faults. Local observations of extensional kinematics are detected, with nodal fault planes consistent with ENE-striking normal faults.

Strike-slip deformation in the arc domain, coherent with ~N-S striking mapped dextral faults, suggests a northward motion of the forearc sliver, accompanied by margin-parallel shortening at its leading edge, *i.e.*, a buttress effect (Beck *et al.,* 1993; Lavenu and Cembrano, 1999; Farías *et al.,* 2006).

4. Discussion

4.1. Exploring the role of margin-parallel *versus* transverse faults on slip partitioning

Subtle but sharp along-strike variations in the continental margin trend affect the magnitude of the strike-slip component derived from the oblique convergence vector (*e.g.,* Stanton-Yonge *et al.,* 2016; Fig. 2). In the end-member scenario of complete slip partitioning (Fig. 1A), where slip at the plate interface exclusively accommodates the margin-normal component of convergence, the total margin-parallel component that should be accommodated by intra-arc faulting is estimated to be ~35 mm/year between 33° and 38° S and ~24 mm/year between 38° and 47° S.

Under a complete partitioning scenario, the slip vectors of subduction earthquakes would be oriented orthogonal to the margin (Beck, 1991; McCaffrey, 1992). However, Stanton-Yonge *et al.* (2016) obtained an average slip direction of N89°E by analyzing 20 subduction earthquakes for the 33-39° S region. This indicates that slip at the plate interface accommodates only part of the oblique convergence, suggesting partial partitioning in this segment (Fig. 1B). The difference between the convergence vector and the thrust earthquake slip vectors leads to a residual slip vector of 13.5 mm/year of margin-parallel displacement, which should be accommodated in the upper plate between 33° and 38° S, and 12.1 mm/year between 38° and 47° S (Fig. 2).

Applying the same analysis to a more recent subduction earthquake that occurred at 43° S (December 2016; Mw 7.6), the slip vector has a trend of N93°E, which is close to the margin-orthogonal orientation (~N100°E). This indicates a more complete partitioning toward the southern end of the study area and, consequently, a larger margin-parallel slip component that must be accommodated within the upper plate (~17 mm/year).

Fault slip estimates at the northern end of the LOFS, whether seismic or aseismic, can reach as high as 18 mm/year (Astudillo-Sotomayor *et al.,* 2021). However, this finding poses a potential inconsistency: even if the single fault examined by Astudillo-Sotomayor *et al.* (2021) accounted for all margin-parallel slip vectors, the slip rate should be only ~13 mm/year, which is the expected end-member of partial partitioning (Stanton-Yonge *et al.,* 2016). Furthermore, because the LOFS consists of multiple subparallel strands, the overall potential slip should be accommodated across multiple faults. It is also important to note that in situ block rotation and permanent distributed strain across the upper plate have been documented, deformation components that also contribute to accommodating the oblique convergence at the plate margin (García *et al.,* 1988; Rojas *et al.,* 1994; Cembrano *et al.,* 2002; Hernández *et al.,* 2014, 2016). A plausible explanation for the unusually high slip rate observed by Astudillo-Sotomayor *et al.* (2021) is that the northward displacement of the forearc sliver, driven by the Chile Ridge subduction at 46° S, may significantly amplify dextral strike-slip along margin-parallel faults (*e.g.,* Forsythe and Nelson, 1985; Cande and Leslie, 1986; Cembrano *et al.,* 2002). On the other hand, at the southernmost segment of the LOFS (~46° S), De Pascale *et al.* (2021) suggested a Quaternary dextral slip rate of 11 to 24 mm/year based on displaced glacial landforms, calculations that, however should be interpreted with caution, as the dates of the glacial landforms are not sufficiently well-constrained.

Regarding the role of margin-parallel versus margin-oblique faults in slip partitioning, transverse faults can effectively accommodate part of the margin-orthogonal component of oblique convergence across the submerged forearc, arc, and back-arc regions (*e.g.,* Sielfeld *et al.* 2019b). This observation supports the concept of kinematic partitioning of overall transpressional deformation at all scales, from regional to local (Fig. 1C). Transverse faults may also accommodate different long- and short-term, along-strike shortening when acting as transfer faults (*e.g.,* Arriagada *et al.* 2000), where faults can switch displacement sense at various time scales.

4.2. The seismic versus aseismic nature of long-term fault slip

While there is a significant spatial correlation between long-term faulting and current crustal earthquakes, the extent to which slip is accommodated through seismic and aseismic processes remains elusive. This uncertainty has important implications for our understanding of fault mechanics in the upper crust and for estimates of a fault's seismic potential.

In the study area, mesoscopic fault surfaces with striae (slickensides) typically show one or more of the following features: ridge-and-groove striae, mineral fibers, mineral precipitation behind fault steps, breccia patches, and gouge (Fig. 5). The widespread presence of mineral fibers behind fault steps rather than bladed calcite (believed to be representative of seismic slip), along with the apparent lack of pseudotachylytes (friction-induced melts), suggests that most of the mapped mesoscopic faults represent aseismic slip.

The debate surrounding whether fault surfaces and their kinematic indicators, as observed in the field, represent seismic slip or slow slip has persisted for decades (Rowe and Griffith, 2015, and references therein). One interpretation of aseismic creep involves mineral fibers and the pressure solution process. Pressure solution is an effective mechanism that dissolves asperities that hinder fault slip and promotes the growth of mineral fibers within fault slip zones (*e.g.,* Gratier and Gamond, 1990; Gratier *et al.,* 2011). It includes successive stages: dissolution, transfer, and deposition, indicating a slow displacement that is not relevant to the dynamic movement of large earthquakes (*e.g.,* Rutter, 1983). However, recent studies suggest that creep processes may not relieve tectonic stress sufficiently to prevent earthquake rupture, and some have even proposed that a creeping fault could still produce large-magnitude earthquakes (*e.g.,* Noda and Lapusta, 2013; Chen and Bürgmann, 2017).

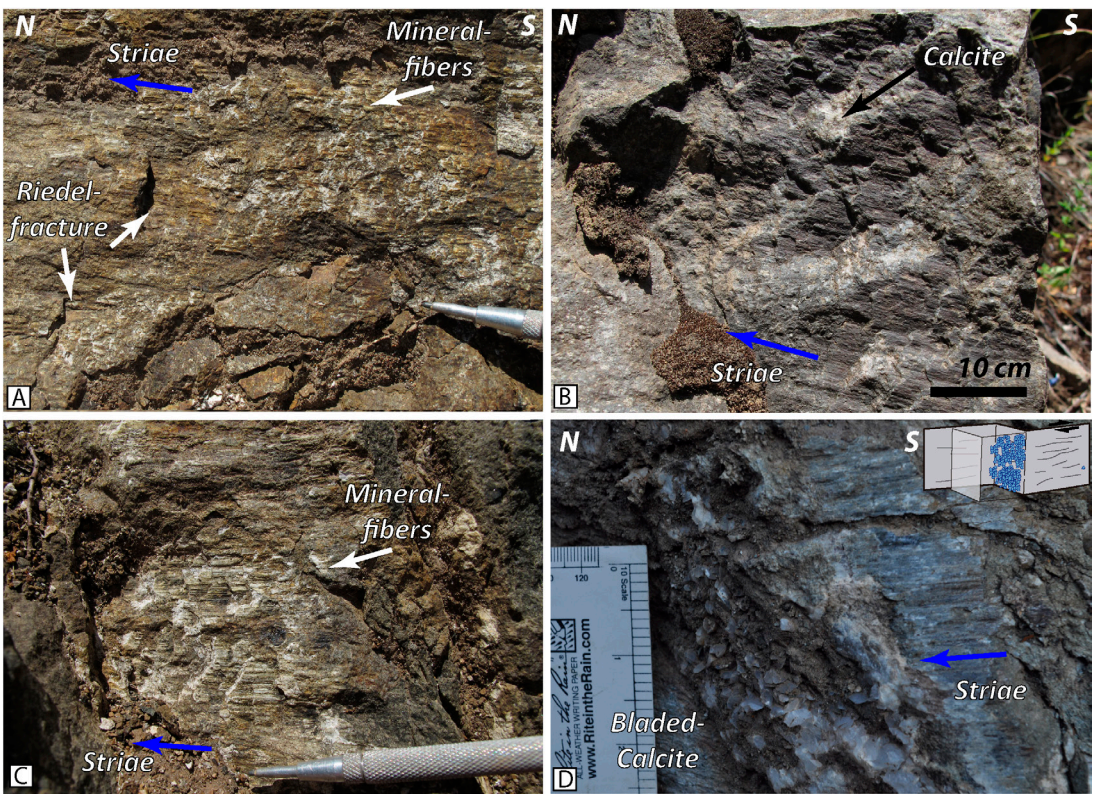

FIG. 5. Typical examples of mesoscopic fault surfaces with striae (slickensides) in the study area. These surfaces exhibit one or more of the following features: **(A)** dextral Riedel-type fractures and mineral fibers; **(B)** calcite precipitation behind fault steps; **(C)** zeolite slickenfibers; and **(D)** bladed-like calcite inside a dilatational jog (diagram provided for spatial context).

The lack of evidence for seismic slip in an exhumed fault zone does not exclude a seismogenic history. For example, pseudotachylytes are among the most reliable indicators of paleo-seismic slip (Rowe and Griffith, 2015). Experimental research indicates that they can form after only millimeters of seismic slip (*e.g.,* Niemeijer *et al.,* 2011), suggesting that they should be common in seismogenic faults. Pseudotachylytes are, however, rarely reported in the literature, possibly due to the difficulty in identifying them (*e.g.,* Kirkpatrick and Rowe, 2013) and their rapid removal from the geological record through hydrothermal alteration (*e.g.,* Fondriest *et al.,* 2020). To our knowledge, with very local exceptions (see bladed calcite in figure 5D), no conclusive seismic markers of any type have been documented along the exhumed outcrops associated with the LOFS. This lack of field evidence, however, does not preclude the LOFS from being seismogenic. In fact, the historic seismicity linked to this fault (Fig. 2) provides clear evidence of its current seismogenic nature, even though seismicity at the LOFS appears scattered and relatively infrequent for a fault that likely accommodates long-term slip rates of up to 20 mm/yr. The apparent mismatch between the fault's activity and its estimated long-term slip rates, combined with evidence in favor of paleo-aseismic slip, suggests that part of the slip may occur without earthquakes (*e.g.,* Astudillo-Sotomayor *et al.,* 2023). A thorough characterization and quantification of the division between seismic and aseismic slip along the LOFS is beyond the scope of this study and would require detailed, long-term geodetic measurements.

4.3. The role of hot fluids in intra-arc brittle deformation

Records of crustal seismicity show more concentrated, intense activity in the intra-arc domain than in the adjacent forearc and back-arc regions (*e.g.,* Weller, 2012). Additionally, whereas crustal seismicity in these latter two regions can reach depths of ~30 km, the typical depth of the crustal seismogenic zone in the intra-arc is ~10 km. The inverse relationship between brittle crustal thickness and the geothermal gradient supports the idea that active magmatic regions experience higher strain rates, promoting feedback between fracturing, increased permeability, and fluid flow (*e.g.,* Rowland and Simmons, 2012). Rock strength decreases when fluids are present within the rock-mass porosity, leading to greater damage under a given far-field differential stress (Lockner, 1995). Conversely, the absence of fluids results in less strain under the same stress regime. Therefore, the combined effect of a thin, brittle volume containing fluid will cause concentrated damage and larger slip magnitudes than those otherwise predicted from mechanical strain partitioning alone. Although no quantitative studies have yet shown the exact amount of slip contributed by these combined factors, we expect it to be on the order of a few millimeters per year.

4.4. Significance of long- and short-term kinematics in the along- and across-strike segmentation of the Southern Andes

Our new and revised compilation of fault slip data, along with crustal earthquake focal mechanisms from global and local networks, provides an improved understanding of the nature of slip partitioning between 33° and 47° S. Four main segments are proposed (Fig. 6):

1. 33-34° S, characterized by a very small oblique convergence angle and no margin-parallel intra-arc faulting. E-W shortening is accommodated by ENE dextral and WNW sinistral strike-slip faults within the arc domain, and by margin-parallel reverse faults in the back-arc (*e.g.,* Ammirati *et al.,* 2022). Deformation in this segment is also characterized by several local Quaternary faults in the forearc and arc regions, consistent with ~N-S shortening (Lavenu and Cembrano, 2008; McKinnon and Garrido de la Barra, 2003). These faults are kinematically consistent with present-day earthquake focal mechanisms (Figs. 2 and 4). The coexistence of ~E-W and ~N-S shortening in this segment can be explained by a radial compression strain/stress field, particularly along the WNW boundary zone (here named the Maipo deformation zone) between segments 1 and 2. The Maipo deformation zone occurs at the Maipo Orocline, and coincides with a regional WNW magnetic anomaly and surface faults (Wall *et al.,* 1996; Yáñez *et al.,* 1998, 2024; Arriagada *et al.,* 2013; Piquer *et al.,* 2021). Radial compression at the southern boundary of this segment was suggested by Allmendinger *et al.* (2006) based on independent GPS and geological data. The Maipo boundary also marks a sharp transition in rock exhumation and an elevation drop of about 2 km in the Main Cordillera (Figs. 2 and 6), also coinciding with a key geological discontinuity where the Frontal Cordillera ends (*e.g.,* Ramos *et al.,* 1986).

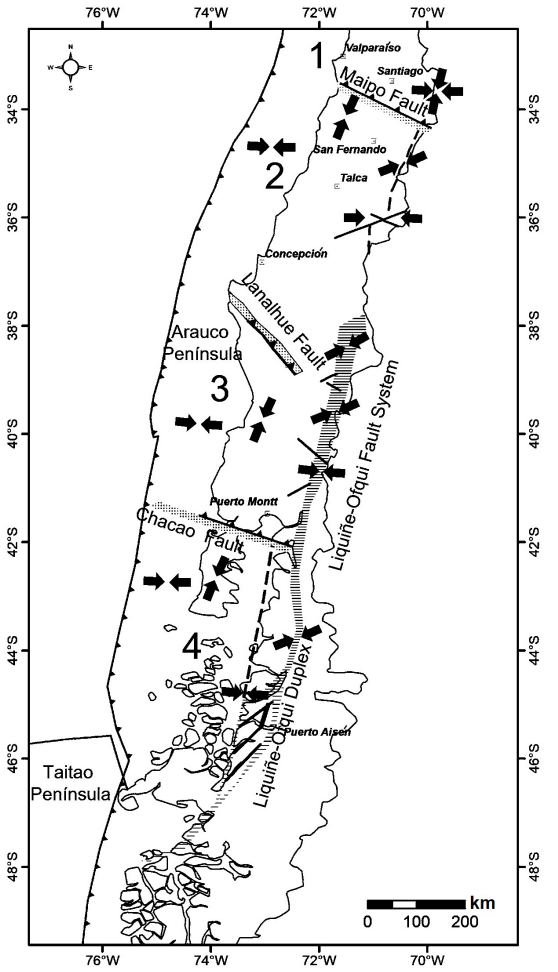

FIG. 6. Summary cartoon illustrating the along- and across-strike segmentation in the geometry and kinematics of slip and deformation partitioning in the Southern Andes. All segments are bounded by south-verging, WNW- to NW-striking reverse faults/deformation zones, namely Maipo, Lanalhue, and Chacao. Black arrows roughly indicate approximate P directions (T axes are not shown for simplicity). The dotted patterns around the major segment boundary faults represent their approximate widths as deformation zones. The striped pattern associated with the LOFS marks the approximate region containing both master and subsidiary faults. See text for details.

2. 34-37° S, characterized by a more pronounced oblique convergence, partitioned into margin-parallel dextral faults and margin-oblique transverse faults. The first ones are mostly blind, *i.e.*, documented almost exclusively by earthquake focal mechanisms, yet with a few exceptions (*e.g.,* the El Melado Fault; Cardona *et al.,* 2018; Sielfeld *et al.,* 2019b). At around 35.5° S, a set of ENE-striking dextral transtensional faults is spatially associated with a marked shift in the location of the present-day volcanic arc front (*e.g.,* Sielfeld *et al.,* 2019b; Ruz-Ginouves *et al.,* 2020). In this segment, a portion of the margin-orthogonal shortening component is accommodated by WNW sinistral transpressional faults and NE dextral faults, of which the former appears to be seismically active (Stanton-Yonge *et al.,* 2016, 2025; Vigide *et al.,* 2025). The boundary between segments 2 and 3 corresponds to a set of NW-striking faults, of which the most prominent is the Lanalhue Fault (*e.g.,* Melnick *et al.,* 2009). This boundary also coincides with significant latitudinal changes in exhumation levels, especially in the forearc region. We propose that this boundary is a crustal-scale, steeply dipping, south-verging reverse fault, in accordance with the work by Melnick *et al.* (2009).

3. 37-41° S. This segment features a well-documented margin-parallel slip component, accommodated by the LOFS and by seismically active NW and NE strike-slip faults. The emerged forearc region is characterized by margin-parallel shortening active since at least the late Pliocene epoch, as suggested by fault slip data and current focal mechanisms. The ~N-S shortening is probably a consequence of a buttress effect acting on the leading edge of the northward-moving forearc sliver (*e.g.,* Beck *et al.,* 1993; Melnick *et al.,* 2009; Astudillo *et al.,* 2023). The southern boundary of this segment is marked by the WNW-striking Chacao Fault System north of Chiloé Island. Surface geology reveals, in this southern end, a contrast in exhumation levels, particularly along the volcanic arc, where mylonites to the north give way to brittle faults to the south (*e.g.,* Cembrano *et al.* 2000).

The LOFS ends as an extensional imbricate fan (horsetail structure) at around 38° S and connects with the Antiñir-Copahue Fault System in the back-arc (Folguera *et al.,* 2004; Melnick *et al.,* 2006; Pérez-Flores *et al.,* 2016). Regardless of how dextral strike-slip motion is accommodated at the northern end of the LOFS, the northward movement of the forearc sliver should decrease to nearly zero at the same latitude. This is because fault displacement should be maximum at the central or trailing segments of any strike-slip fault, naturally tapering off approaching their leading edge, especially when they are buttressed (*e.g.,* Beck *et al.,* 1993). This creates a latitudinal

displacement gradient, resulting in margin-parallel shortening of the forearc accompanied by counterclockwise tectonic rotation (*e.g.,* Hernández-Moreno, 2014, 2016). Margin-parallel shortening has also been observed in the forearc of northern Chile (González *et al.,* 2008; Allmendinger and González, 2010), where conspicuous E-W faults are currently active. A similar pattern of margin-parallel shortening and block rotation has been found in the forearc of Cascadia (*e.g.,* Johnson *et al.,* 2004). In Cascadia, as well as in the Southern Andes, roughly E-W margin-normal compression dominates the forearc region near the trench, where the plates appear to be locked. In contrast, when slow slip and tectonic tremors dominate the subduction interface, and the plates are less strongly coupled, the forearc begins to accommodate the margin-parallel shortening through strike-slip and thrust at transverse crustal faults (*e.g.,* Balfour *et al.,* 2011).

4. 41-47° S. This segment accommodates most of the upper plate deformation through a transtensional strike-slip duplex composed of two right-stepping margin-parallel dextral strike-slip faults joined by NE-trending normal and dextral-normal faults (Cembrano *et al.,* 1996). Fault-slip data and earthquake focal mechanisms are internally consistent with the long-term kinematics of the LOFS (Arancibia *et al.,* 1999; Lavenu and Cembrano, 1999; Cembrano *et al.,* 2002; Pérez-Estay *et al.,* 2020). The northward, margin-parallel motion of the forearc sliver is strongly supported by geological, geodetic, paleomagnetic, and seismological data (Beck *et al.,* 1993; Rojas *et al.,* 1994; Cembrano *et al.,* 2000; Wang *et al.,* 2007; Melnick *et al.,* 2009; Moreno *et al.,* 2016; Sielfeld *et al.,* 2019a).

Tectonic boundaries between segments 1-2 and 2-3 are interpreted in this work as major, deep-seated south-verging reverse faults. The boundary between segments 3-4 is also a crustal-scale fault, although there is no clear evidence of vergence. Based on geological mapping and geophysical evidence, Yáñez *et al.* (2024) identified these features as first-order, long-lived tectonic structures, likely active since at least the Permo-Triassic. During the Neogene-Quaternary, these faults have influenced the location of volcanic alignments and ore deposits in the arc domain (*e.g.,* Lara *et al.,* 2004; Cembrano and Lara, 2009; Piquer *et al.,* 2015).

4.5. Implications for seismic hazard

Local paleo-seismological, geophysical, and morphological studies focused on specific fault strands have provided estimates of their geometry, kinematics, and recurrence intervals for the studied area Notable examples include the works of Vargas *et al.* (2014) and Yáñez *et al.* (2020) on the west-verging, reverse San Ramon Fault in the Andean foothills of Santiago (33.5° S), with slip rates estimated between 0.3-0.5 mm/year. At around 36° S, Vega-Ruiz *et al.* (2025) investigated Quaternary deformation along the western margin of the Main Cordillera driven by west-verging reverse faults, obtaining slip rates of up to 0.58 mm/year and estimated a maximum Mw of 7.0. Further south, in the LOFS domain, morphotectonic analyses of well-exposed master and splay faults have revealed slip rates of 10-22 mm/year (Astudillo *et al.,* 2018, 2021, 2023; De Pascale *et al.* 2021), significantly higher when compared to estimates in the north. However, smaller slip-rate values are obtained from numerical modeling: 1 to 7 mm/year for the margin-parallel LOFS, ~1 mm/year for the Andean transverse faults, and 5-10 mm/year along the southern master faults of the LOFS (*e.g.,* Stanton-Yonge *et al.,* 2016; Iturrieta *et al.,* 2017).

While these studies have greatly enhanced our understanding of seismic hazards in Chile, there has been a lack of systematic efforts to contextualize the fault systems within a broader tectonic framework. Specifically, there has been insufficient discussion of their role in plate margin partitioning and of the interplay between the seismic and aseismic components of the reported fault displacements. Moreover, long-term evidence of fault slip for many of these potentially hazardous faults has not been critically integrated into the discussion surrounding the primary geological processes involved, complicating comparisons with short-term deformation observations. However, compilations focused on the nature and spatial distribution of Quaternary crustal faults in the studied region (*e.g.,* Lavenu *et al.,* 2000; Santibáñez *et al.,* 2019; Maldonado *et al.,* 2021) are available, while Costa *et al.* (2020) presented a compilation of Quaternary faults for South America and provided an estimation of the regional-scale seismic hazard.

In terms of seismic hazard, our synthesis of crustal seismicity and long-term fault-slip data suggests the following:

Aseismic slip should be considered when interpreting data from morphotectonic analyses and

fault separation of markers in potentially seismogenic faults (*e.g.,* LOFS). In fact, Astudillo *et al.* (2023) observed a discrepancy between their estimated slip rates and the recurrence times of historical earthquakes in the LOFS, with aseismic slip required to reconcile the two. This observation is consistent with long-term evidence of displacement in mesoscopic faults within the same fault systems where Holocene fault slip estimates have been made, indicating that these faults exhibit a significant amount of aseismic slip, as demonstrated by the presence of slickenfibers on fault surfaces and shear bands, which are commonly used as kinematic indicators (*e.g.,* Pérez-Flores *et al.* 2016). Evidence for seismic slip in fossil faults is often elusive (*e.g.,* Rowe and Griffith, 2015), and only specific microstructures indicate dynamic rupturing. The primary implication of the above points is that many morphotectonic and paleo-seismological studies may significantly overestimate seismic fault-slip rates, thereby exaggerating deterministic estimates of earthquake magnitudes (*e.g.,* Burgmann, 2018).

The tectonic transitions between the proposed segments identified in this study are likely to play (and have played) a crucial role in the seismo-tectonic segmentation of the margin. For instance, Yáñez *et al.* (2024) suggested that trans-lithospheric faults have acted as regions of weak coupling, functioning as long-term, geologically controlled seismic barriers. The release of fluids from the Wadati-Benioff zone could be the driving force behind this creep-like mechanism. Ample evidence of reverse faulting in these boundary zones is a key factor in understanding these potential seismic barriers.

In probabilistic seismic hazard analysis (PSHA; *e.g.,* Gerstenberger *et al.,* 2020), the contribution of crustal faults should be evaluated alongside the dominant subduction interface hazard. In addition, because crustal sources are typically shallow and near the sites of analysis, they can locally elevate seismic hazard within a narrow spatial range. In the near-fault region, the long-return-period tail of the hazard curve can be controlled by the fault itself, even when its occurrence rates are low (*e.g.,* Youngs and Coppersmith, 1985; Baker, 2013). In our compiled instrumental catalog, the maximum documented magnitudes for intra-arc events are Mw 6.5 in the north and Mw 6.2 in the south. Traditional PSHA studies complement seismicity observations by constraining the maximum magnitude and the magnitude-frequency distribution using mapped fault geometries and slip rates (*e.g.,* Gerstenberger *et al.,* 2020). Despite notable efforts to characterize faults in Chile (*e.g.,* Santibáñez *et al.,* 2019; Maldonado *et al.,* 2021), further work is needed to determine slip rates across all seismogenic faults in a harmonized, systematic manner (*e.g.,* Seebeck *et al.,* 2023; Basili *et al.,* 2024). Future PSHA would certainly benefit from more accurate estimates on interseismic slip rates from geodesic and remote sensing data (*e.g.,* Chaussard *et al.,* 2016), along with physics-based rupture models, to explore the seismic potential of crustal faults, including the contribution of slow slip to the earthquake cycle (*e.g.,* Bürgmann, 2018). For instance, dense, near-fault Global Navigation Satellite System surveys could geodetically constrain interseismic strain, steady creep, and/or transient slow-slip events (*e.g.,* Rousset, 2019), thereby better constraining the seismic slip deficit relevant for hazard assessment.

5. Conclusions

The combination of new and unpublished fault-slip data, and of regional and local crustal seismicity, enables an updated understanding of the geometry and kinematics of slip partitioning along and across the South American plate boundary between 33° and 47° S. This partitioning proves to be much more complex than previously thought, with implications for plate-margin tectonics, the spatial and temporal distribution of fault slip, and interactions with other processes such as active faulting and volcanism.

Slight variations in the along-strike orientation of the continental margin influence different stress and strain distributions. Radial shortening (constriction) dominates the Maipo Orocline region between 33° and 34° S, as margin-orthogonal and margin-parallel shortening spatially coincide in a zone where there is a transition from non-partitioned to partitioned deformation. Another important change occurs at around 37° S, where the strike-slip component of the convergence vector is reduced, and the transcurrent margin-parallel slip is absorbed by a major, continuous intra-arc fault system, the LOFS, between 37° and 46° S. Region-wide, the predominantly E-W shortening documented in the submarine forearc contrasts with the margin-parallel shortening observed from seismicity and fault slip data along the emerged forearc region. In the arc domain, a combination of E-W shortening and NE-SW shortening, the latter accommodated by a mostly hidden dextral fault between 34° and 37° S, is then replaced to the south by a continuous surface expression of dextral

faulting and transverse, seismically active NE and NW dextral and sinistral faults.

The forearc sliver between 33° and 47° S is divided into four main blocks, separated by prominent WNW- to NW-striking fault zones that may or may not extend into the volcanic arc region. At the Maipo Orocline zone, a WNW transverse deformation zone/fault places deeper crustal levels in the north over shallower levels in the south, indicating a predominantly south-verging reverse fault or deformation zone. Surface faults, such as Melipilla, Piuquencillo, and Pichilemu, are believed to be surface expressions of this WNW deformation boundary. Farther south, at the Arauco Peninsula region, where the continental margin shifts from a NNE to a ~N-S orientation, another major NW-striking boundary separates Silurian-to-Permian metamorphic rocks and intrusives to the north from mostly Paleozoic metamorphic rocks to the south. As noted in previous works, this boundary is represented at the surface by the NW-striking, south-verging Lanalhue reverse fault, which tends to fade toward the volcanic arc. The fourth and last crustal block lies south of the WNW-striking, mostly reverse, south-verging Chacao Fault, and is dominated by the LOFS strike-slip duplex as the main tectonic element, which mostly accommodates dextral strike-slip deformation.

Finally, in the LOFS, evidence for mostly slow slip (observed on exhumed striated fault surfaces from where instantaneous shortening and extension axes were derived) challenges the idea that these mesoscopic faults are fossil earthquake sites and raises questions about whether seismic events are always the source of the morphological and stratigraphic evidence of slip. It is therefore very likely that calculated slip rates overestimate the seismic slip budget, thereby affecting seismic hazard assessments.

Acknowledgements

The senior authors of this paper would like to warmly thank Francisco Hervé for inspiring us in our early stages as independent researchers. This paper is dedicated to him. Pancho introduced us to the Liquiñe-Ofqui Fault System in the late 1980s, and from then on, it has captivated our interest and encouraged us to go further than previous generations, along with many bright students, our junior coauthors, who are now moving the frontiers of science. Numerous Fondecyt projects have generously supported most of the research shown in this paper over the last few decades. The first of these, headed by Pancho, was also supported by later projects shared with F. Munizaga, L. Lara, H. Moreno, L. López-Escobar, among several others. The Andean Geothermal Center of Excellence, led by D. Morata and beginning in 2001, significantly advanced work in key areas of the Southern Andes. We sincerely thank our friends L. Lara and G. González for the many insightful discussions we have had over the years on the topics covered in this paper. Many M.Sc. and Ph.D. ANID scholarships provided crucial funding for the junior co-authors to develop innovative ideas on various topics related to slip partitioning, using a combination of traditional geological and geophysical techniques and cutting-edge numerical modeling.

A. Lavenu's stay in Chile was funded by ORSTOM and later by IRD for several years. This marked the start of research on the kinematic analysis of fault surfaces and how this knowledge was passed down through generations in Chile.

C. Rojas and J. Cembrano would like to thank Prof. Myrl Beck from Western Washington University, who introduced them to the concept of slip partitioning and paleomagnetism at convergent margins in the early 1990s. He is no longer with us, but his passion for tectonic processes lives on in our hearts.

The manuscript was greatly improved thanks to the helpful comments from reviewers K. Klepeis and C. Canora. We are especially grateful to Guest Editor R. Pankhurst for his patient review, thoughtful editing, and careful handling of the manuscript. Journal Editor D. Bertin thoroughly reviewed the latest revised version of the manuscript. Lastly, we sincerely thank M. Calderón for encouraging us to submit our work to this special issue.

Data and Resources

The GCMT (https://www.globalcmt.org/; Ekström *et al.,* 2012) and ANSS-ComCat (https://earthquake.usgs.gov/; USGS, 2017) catalogs were last accessed on August 1, 2025. Local-network hypocenters and focal mechanisms were compiled from the published studies cited in the text. Slab geometry was obtained from the Slab2 model (Hayes *et al.,* 2018). Data processing and catalog merging/classification were performed in Python, with the assistance of the obspy (Beyreuther *et al.,* 2010), pycsep (Savran *et al.,* 2022), mplstereonet (https://pypi.org/project/mplstereonet/), and FMC (Alvarez-Gómez, 2019) packages. Fault-slip kinematic summaries and stereonets were generated with

FaultKin (Allmendinger *et al.,* 2012). The final maps were prepared in QGIS (https://www.qgis.org). All collected catalogs, fault kinematic measurements, and the derived and processed datasets are archived in the accompanying Zenodo repository: https://zenodo.org/records/17296705.

References

Agurto, H.; Rietbrock, A.; Barrientos, S.; Bataille, K.; Legrand, D. 2012. Seismotectonic structure of the Aysén Region, Southern Chile, inferred from the 2007 Mw=6.2 Aysén earthquake sequence. Geophysical Journal International 190 (1): 116-130. https://doi.org/10.1111/j.1365-246X.2012.05507.x

Agurto-Detzel, H.; Rietbrock, A.; Bataille, K.; Miller, M.; Iwamori, H.; Priestley, K. 2014. Seismicity distribution in the vicinity of the Chile Triple Junction, Aysén Region, southern Chile. Journal of South American Earth Sciences 51: 1-11. https://doi.org/10.1016/j.jsames.2013.12.011

Allmendinger, R.W.; González, G. 2010. Invited review paper: Neogene to Quaternary tectonics of the coastal Cordillera, northern Chile. Tectonophysics 495 (1-2): 93-110. https://doi.org/10.1016/j.tecto.2009.04.019

Allmendinger, R.; Yáñez, G.; Cembrano, J. 2006. Instantaneous deformation associated with flat subduction: Insights from GPS strain rates and numerical modelling. *In* Congreso Geológico Chileno, No. 11, Actas 1: 367-370. Antofagasta.

Allmendinger, R.W.; Cardozo, N.C.; Fisher, D. 2012. Structural Geology Algorithms: Vectors and Tensors. Cambridge University Press: 289 p. https://doi.org/10.1017/CBO9780511920202

Álvarez-Gómez, J.A. 2019. FMC-Earthquake focal mechanisms data management, cluster and classification. SoftwareX 9: 299-307. https://doi.org/10.1016/j.softx.2019.03.008

Ammirati, J-B.; Vargas, G.; Rebolledo, S.; Abrahami, R.; Potin, B; Leyton, F.; Ruiz, S. 2019. The crustal seismicity of the Western Andean Thrust (Central Chile, 33º-34ºS): implications for regional tectonics and seismic hazard in the Santiago area. Bulletin of the Seismological Society of America 109 (5): 1985-1999. https://doi.org/10.1785/0120190082

Ammirati, J-B.; Villaseñor, A.; Chevrot, S.; Easton, G.; Lehujeur, M.; Ruiz, S.; Flores, M.C. 2022. Automated earthquake detection and local travel time tomography in the South-Central Andes (32-35ºS): Implications for regional tectonics. Journal of Geophysical Research, Solid Earth 127 (4). https://doi.org/10.1029/2022JB024097

Angermann, D.; Klotz, J.; Reigber, C. 1999. Space-geodetic estimation of the Nazca-South America Euler vector. Earth and Planetary Sciences Letters 171 (3): 329-334. https://doi.org/10.1016/S0012-821X(99)00173-9

Arancibia, G.; Cembrano, J.; Lavenu, A. 1999. Transpresión dextral y partición de la deformación en la Zona de Falla Liquiñe-Ofqui, Aisén, Chile (44-45ºS). Revista Geológica de Chile 26 (1): 3-22. http://dx.doi.org/10.4067/S0716-02081999000100001

Aron, F.; Allmendinger, R.W.; Cembrano, J.; González, G.; Yáñez, G. 2013. Permanent fore-arc extension and seismic segmentation: Insights from the 2010 Maule earthquake, Chile. Journal of Geophysical Research, Solid Earth 118 (2): 724-739. https://doi.org/10.1029/2012JB009339

Arriagada, C.; Roperch, P.; Mpodozis, C. 2000. Clockwise block rotations along the eastern border of the Cordillera de Domeyko, Northern Chile (22º45'-23º30' S). Tectonophysics 326 (1-2): 153-171. https://doi.org/10.1016/S0040-1951(00)00151-7

Arriagada, C.; Ferrando, R.; Córdova, L.; Morata, D.; Roperch, P. 2013. The Maipo Orocline: A first scale structural feature in the Miocene to Recent geodynamic evolution in the central Chilean Andes. Andean geology 40 (3): 419-437. http://dx.doi.org/10.5027/andgeoV40n3-a02

Astudillo, L.; Cortés-Aranda, J.; Melnick, D.; Tassara, A. 2018. Holocene deformation along the Liquiñe-Ofqui Fault Zone, southern Chile: Field observations and geomorphic analysis. In International INQUA Meeting on Paleoseismology, Active Tectonics and Archeoseismology (PATA), No. 9. Possidi.

Astudillo-Sotomayor, L.; Jara-Muñoz, J.; Melnick, D.; Cortés-Aranda, J.; Tassara, A.; Strecker, M.R. 2021. Fast Holocene slip and localized strain along the Liquiñe-Ofqui strike-slip fault system, Chile. Scientific Reports 11. https://doi.org/10.1038/s41598-021-85036-5

Astudillo-Sotomayor, L.; Cortés-Aranda, J.; Melnick, D.; Jara-Muñoz, J.; Cabello, C.; Perucca, L.; Tassara, A.; Pérez-Peña, J. V.; León-Ibáñez, P. 2023. Neotectonic faults in the Southern Chile intra-arc (38º S-40.5º S): Insights about their seismic potential and the link with the megathrust earthquake cycle. Tectonophysics 846. https://doi.org/10.1016/j.tecto.2022.229675

Baker, J.W. 2013. Probabilistic seismic hazard analysis. White Paper Version 2.0.1: 79 p.

Balfour, N.J.; Cassidy, J.F.; Dosso, S.E.; Mazzotti, S. 2011. Mapping crustal stress and strain in southwest British Columbia. Journal of Geophysical Research, Solid Earth 116 (B3): 1-11. https://doi.org/10.1029/2010JB008003

Barrientos, S.E.; Acevedo-Aránguiz, P.S. 1992. Seismological aspects of the 1988-1989 Lonquimay (Chile) volcanic

eruption. Journal of Volcanology and Geothermal Research 53 (1-4): 73-87. https://doi.org/10.1016/0377-0273(92)90075-o

Basili, R.; Danciu, L.; Beauval, C.; Sesetyan, K.; Pires Vilanova, S.; Adamia, S.; Arroucau, P.; Atanackov, J.; Baize, S.; Canora, C.; Caputo, R.; Cosimo Carafa, M.M.; Cushing, E.M.; Custódio, S.; Demircioglu Tumsa, M.B.; Duarte, J.C.; Ganas, A.; García-Mayordomo, J.; Gómez de la Peña, J.; Gràcia, E.; Jamsek Rupnik, P.; Jomard, H.; Kastelic, V.; Maesano, F.E.; Martín-Banda, R.; Martínez-Loriente, S.; Neres, M.; Perea, H.; Sket Motnikar, B.; Tiberti, M.M.; Tsereteli, N.; Tsironi, V.; Vallone, R.; Vanneste, K.; Zupancic, P.; Giardini, D. 2024. The European fault-source model 2020 (EFSM20): Geologic input data for the European Seismic Hazard Model 2020. Natural Hazards and Earth System Sciences 24 (11): 3945-3976. https://doi.org/10.5194/nhess-24-3945-2024

Beck, M.E. Jr. 1991. Coastwise transport considered: Lateral displacements in oblique subduction zones, and tectonic consequences. Physics of the Earth and Planetary Interiors 68: 1-8. https://doi.org/10.1016/0031-9201(91)90002-Y

Beck, M.E. Jr.; Rojas, C.; Cembrano, J. 1993. On the nature of buttressing in margin-parallel strike-slip fault systems. Geology 21 (8): 755-758. https://doi.org/10.1130/0091-7613(1993)021%3C0755:OTNOBI%3E2.3.CO;2

Beyreuther, M.; Barsch, R.; Krischer, L.; Megies, T.; Behr, Y.; Wassermann, J. 2010. ObsPy: A Python toolbox for seismology. Seismological Research Letters 81 (3): 530-533. https://doi.org/10.1785/gssrl.81.3.530

Bravo, F.; Koch, P.; Riquelme, S.; Fuentes, M.; Campos, J. 2019. Slip distribution of the 1985 Valparaíso earthquake constrained with seismic and deformation data. Seismological Research Letters 90 (5): 1792-1800. https://doi.org/10.1785/0220180396

Bürgmann, R. 2018. The geophysics, geology and mechanics of slow fault slip. Earth and Planetary Science Letters 495 (1): 112-134. https://doi.org/10.1016/j.epsl.2018.04.062

Cande, S.C.; Leslie, R.B. 1986. Late Cenozoic tectonics of the Southern Chile Trench. Journal of Geophysical Research, Solid Earth 91 (B1): 471-496. https://doi.org/10.1029/JB091iB01p00471

Canora, C.; Martínez-Díaz, J.; Villamor, P.; Staller, A.; Berryman, K.; Álvarez-Gómez, J.A.; Capote, R.; Diaz, M. 2014. Structural evolution of the El Salvador Fault Zone: An evolving fault system within a volcanic arc. Journal of Iberian Geology 40 (3): 471-488. https://doi.org/10.5209/rev_JIGE.2014.v40.n3.43559

Cardona, C.; Tassara, A.; Gil-Cruz, F.; Lara, L.; Morales, S.; Kohler, P.; Franco, L. 2018. Crustal seismicity associated to rapid surface uplift at Laguna del Maule Volcanic Complex, Southern Volcanic Zone of the Andes. Journal of Volcanology and Geothermal Research 353: 83-94. https://doi.org/10.1016/j.jvolgeores.2018.01.009

Cembrano, J.; Lara, L. 2009. The link between volcanism and tectonics in the southern volcanic zone of the Chilean Andes: A review. Tectonophysics 471 (1-2): 96-113. https://doi.org/10.1016/j.tecto.2009.02.038

Cembrano, J.; Hervé, F.; Lavenu, A. 1996. The Liquiñe Ofqui fault zone: a long-lived intra-arc fault system in southern Chile. Tectonophysics 259 (1-3): 55-66. https://doi.org/10.1016/0040-1951(95)00066-6

Cembrano, J.; Schermer, E.; Lavenu, A.; Sanhueza, A. 2000. Contrasting nature of deformation along an intra-arc shear zone, the Liquiñe-Ofqui fault zone, southern Chilean Andes. Tectonophysics 319 (2): 129-149. https://doi.org/10.1016/S0040-1951(99)00321-2

Cembrano, J.; Lavenu, A.; Reynolds, P.; Arancibia, G.; López, G.; Sanhueza, A. 2002. Late Cenozoic transpressional ductile deformation north of the Nazca-South America-Antarctica triple junction. Tectonophysics 354 (3-4): 289-314. https://doi.org/10.1016/S0040-1951(02)00388-8

Charrier, R.; Baeza, O.; Elgueta, S.; Flynn, J.J.; Gans, P.; Mahlburg Kay, S. ; Muñoz, N. ; Wyss, A.R. ; Zurita, E. 2002. Evidence for Cenozoic extensional basin development and tectonic inversion south of the flat-slab segment, southern Central Andes, Chile (33ºS-36ºS.L.). Journal of South American Earth Sciences 15 (1): 117-139. https://doi.org/10.1016/S0895-9811(02)00009-3

Chaussard, E.; Bürgmann, R.; Fattahi, H.; Johnson, C.W.; Nadeau, R.M. 2016. Potential and limits of InSAR to characterize interseismic deformation independently of GPS data: Application to the southern San Andreas Fault system. Geochemistry, Geophysics, Geosystems 17 (3): 1214-1229. https://doi.org/10.1002/2015GC006246

Chen, K.H.; Bürgmann, R. 2017. Creeping faults: good news, bad news? Reviews of Geophysics 55 (2): 282-286. https://doi.org/10.1002/2017RG000565

Chinn, D.S.; Isacks, B.I. 1983. Accurate source depths and focal mechanisms of shallow earthquakes in western South America and in the New Hebrides Island arc. Tectonics 2 (6): 529-563. https://doi.org/10.1029/TC002i006p00529

Costa, C.; Alvarado, A.; Audemard, F.; Audin, L.; Benavente, C.; Hilario Bezerra, F.; Cembrano, J.; González, G.; López, M.; Minaya, E.; Santibáñez, I.; García J.; Acrila, M.; Pagani, M.; Pérez, I.; Delgado, F.; Paolini, M.; Garro, H. 2020. Hazardous faults of South America; compilation and overview. Journal of South

American Earth Sciences 104. https://doi.org/10.1016/j.jsames.2020.102837

De Pascale, G.; Froude, M.; Penna, I.; Hermanns, R.L.; Sepúlveda, S.A.; Moncada, D.; Persico, M.; Easton, G.; Villalobos, A.A.; Gutiérrez, F. 2021. Liquiñe-Ofqui's fast slipping intra-volcanic arc crustal faulting above the subducted Chile Ridge. Scientific Reports 11. https://doi.org/10.1038/s41598-021-03919-z

De Saint Blanquat, M.; Tikoff, B.; Teyssier, C.; Vigneresse, J.L. 1998. Transpressional kinematics and magmatic arcs. Geological Society, London, Special Publications 135: 327-340. https://doi.org/10.1144/GSL.SP.1998.135.01.21

Eisermann, J.O.; Göllner, P.L.; Riller, U. 2021. Orogen-scale transpression accounts for GPS velocities and kinematic partitioning in the Southern Andes. Communications Earth & Environment 2. https://doi.org/10.1038/s43247-021-00241-4

Ekström, G.; Nettles, M; Dziewońsk, A.M. 2012. The global CMT project 2004-2010: Centroid-moment tensors for 13,017 earthquakes. Physics of the Earth and Planetary Interiors 200-201: 1-9. https://doi.org/10.1016/j.pepi.2012.04.002

Farías, M.; Comte, D.; Charrier, R. 2006. Sismicidad superficial en Chile central: Implicancias para el estado cortical y crecimiento de los Andes Centrales australes. *In* Congreso Geológico Chileno, No. 11, Actas 1: 403-406. Antofagasta.

Farías, M.; Charrier, R.; Carretier, S.; Martinod, J.; Fock, A.; Campbell, D.; Cáceres, J.; Comte, D. 2007. Late Miocene high and rapid surface uplift and its erosional response in the Andes of central Chile (33ºS-35ºS). Tectonics 27 (1): 1-22. https://doi.org/10.1029/2006TC002046

Farías, M.; Comte, D.; Roecker, S.; Carrizo, D.; Pardo, M. 2011. Crustal extensional faulting triggered by the 2010 Chilean earthquake: The Pichilemu Seismic Sequence. Tectonics 30 (6): 1-11. https://doi.org/10.1029/2011TC002888

Fitch, T.J. 1972. Plate convergence, transcurrent fault, and internal deformation adjacent to Southeast Asia and the Western Pacific. Journal of Geophysical Research 77 (23): 4432-4460. https://doi.org/10.1029/JB077i023p04432

Folguera, A.; Ramos, V.A.; Melnick, D. 2002. Partición de la deformación en la zona del arco volcánico de los Andes neuquinos (36-39ºS) en los últimos 30 millones de años. Revista Geológica de Chile 29 (2): 151-165. http://dx.doi.org/10.4067/S0716-02082002000200005

Folguera, A.; Ramos, V.A.; Hermanns, R.L.; Naranjo, J. 2004. Neotectonics in the foothills of the southernmost central Andes (37º-38ºS): evidence of strike-slip displacement along the Antiñir-Copahue fault zone. Tectonics 23 (5): 1-23. https://doi.org/10.1029/2003TC001533

Folguera, A.; Introcaso, A.; Gimenez, M.E.; Ruiz, F.; Martinez, M.P.; Tunstall, C.; Garcia Morabito, E.; Ramos, V.A. 2007. Crustal attenuation in the Southern Andean retroarc (38º-39º30'S) determined from tectonic and gravimetric studies: The Lonco-Luán asthenospheric anomaly. Tectonophysics 439 (1-4): 129-147. https://doi.org/10.1016/j.tecto.2007.04.001

Fondriest, M.; Mecklenburgh, J.; Passelegue, F.X.; Artioli, G.; Nestola, F.; Spagnuolo, E.; Rempe, M.; Di Toro, G. 2020. Pseudotachylyte alteration and the rapid fade of earthquake scars from the geological record. Geophysical Research Letters 47 (22): 1-9. https://doi.org/10.1029/2020GL090020

Forsythe, R.; Nelson, E. 1985. Geological manifestations of ridge collision: Evidence from the Golfo de Penas-Taitao Basin, Southern Chile. Tectonics 4 (5): 477-495. https://doi.org/10.1029/TC004i005p00477

Galland, O.; Hallot, E.; Cobbold, P.R.; Ruffet, G.; d'Ars, J.d.B. 2007. Volcanism in a compressional Andean setting: A structural and geochronological study of Tromen volcano (Neuquén province, Argentina). Tectonics 26 (4): 1-24. https://doi.org/10.1029/2006TC002011

García, A.R.; Beck, M.E.; Burmester, R.F.; Munizaga, F.E.; Hervé, F. 1988. Paleomagnetic reconnaissance of the Region de Los Lagos, Southern Chile, and its tectonic implications. Revista Geológica de Chile 15 (1): 13-30.

Gerbault, M.; Cembrano, J.; Mpodozis, C.; Farías, M.; Pardo, M. 2009. Continental margin deformation along the Andean subduction zone: Thermo-mechanical models. Physics of the Earth and Planetary Interiors 177 (3-4): 180-205. https://doi.org/10.1016/j.pepi.2009.09.001

Gerstenberger, M.C.; Marzocchi, W.; Allen, T.; Pagani, M.; Adams, J.; Danciu, L.; Field, E.H.; Fujiwara, H.; Luco, N.; Ma, K.-F.; Meletti, C.; Petersen, M.D. 2020. Probabilistic seismic hazard analysis at regional and national scales: State of the art and future challenges. Reviews of Geophysics 58 (2). https://doi.org/10.1029/2019RG000653

Gerstenberger, M.C.; Bora, S.; Bradley, B.A.; DiCaprio, C.; Kaiser, A.; Manea, E.F.; Nicol, A.; Rollins, C.; Stirling, M.W.; Thingbaijam, K.K.S.; Van Dissen, R.J.; Abbott, E.R.; Atkinson, G.M.; Chamberlain, C.; Christophersen, A.; Clark, K.; Coffey, G.L.; de la Torre, C.A.; Ellis, S.M.; Fraser, J.; Graham, K.; Griffin, J.; Hamling, I.J.; Hill, M.P.; Howell, A.; Hulsey, A.; Hutchinson, J.; Iturrieta, P.; Johnson, K.M.; Oakley Jurgens, V.; Kirkman, R.; Langridge, R.M.; Lee, R.L.; Litchfield, N.L.; Maurer, J.; Milner, K.R.; Rastin, S.; Rattenbury, M.S.; Rhoades, D.A.; Ristau, J.; Schorlemmer, D.; Seebeck, H.; Shaw, B.E.; Stafford, P.J.;

Stolte, A.C.; Townend, J.; Villamor, P.; Wallace, L.M.; Weatherill, G.; Williams, C.A.; Wotherspoon, L.M. 2024. The 2022 Aotearoa New Zealand national seismic hazard model: Process, overview, and results. Bulletin of the Seismological Society of America 114 (1): 7-36. https://doi.org/10.1785/0120230182

Giambiagi, L.B.; Ramos, V.A. 2002. Structural evolution of the Andes in a transitional zone between flat and normal subduction (33º30'-33º45'S), Argentina and Chile. Journal of South American Earth Sciences 15 (1): 101-116. https://doi.org/10.1016/S0895-9811(02)00008-1

Giambiagi, L.; Mescua, J.; Bechis, F.; Tassara, A.; Hoke, G. 2012. Thrust belts of the southern Central Andes: Along-strike variations in shortening, topography, crustal geometry, and denudation. Geological Society of America Bulletin 124 (7-8): 1339-1351. https://doi.org/10.1130/B30609.1

Glodny, J.; Echtler, H.; Collao, S.; Ardiles, M.; Burón, P.; Figueroa, O. 2008. Differential Late Paleozoic active margin evolution in South-Central Chile (37ºS-40ºS) -The Lanalhue Fault Zone. Journal of South American Earth Sciences 26 (4): 397-411. https://doi.org/10.1016/j.jsames.2008.06.001

González, G.; Allmendinger, R.; Dunai, T.; Cembrano, J.; Martinod, J.; Rémy, D.; Carrizo, D.; Loveless, J.P.; Veloso, E.E.; Aron, F.; Cortés-Aranda, J. 2008. The active upper plate deformation of the Central Andes forearc, northern Chile: the geological view. *In* International Symposium on Andean Geodynamics (ISAG), No. 7, Extended Abstracts: 116-119. Nice.

Gratier, J.P.; Gamond, J.F. 1990. Transition between seismic and aseismic deformation in the upper crust. Geological Society, London, Special Publications 54: 461-473. https://doi.org/10.1144/GSL.SP.1990.054.01.42

Gratier, J.P.; Richard, J.; Renard, F.; Mittempergher, S.; Doan, M.L.; Di Toro, G.; Hadizadeh, J.; Boullier, A.M. 2011. Aseismic sliding of active faults by pressure solution creep: Evidence from the San Andreas Fault Observatory at depth. Geology 39 (12): 1131-1134. https://doi.org/10.1130/G32073.1

Hayes, G.P.; Moore, G.L.; Portner, D.E.; Hearne, M.; Flamme, H.; Furtney, M.; Smoczyk, G.M. 2018. Slab2, a comprehensive subduction zone geometry model. Science 362 (6410): 58-61. https://doi.org/10.1126/science.aat4723

Hernández-Moreno, C.; Speranza, F.; Di Chiara, A. 2014. Understanding kinematics of intra-arc transcurrent deformation: Paleomagnetic evidence from the Liquiñe-Ofqui fault zone (Chile, 38-41ºS). Tectonics 33 (10): 1964-1988. https://doi.org/10.1002/2014TC003622

Hernández-Moreno, C.; Speranza, F.; Di Chiara, A. 2016. Paleomagnetic rotation pattern of the southern Chile fore-arc sliver (38° S-42° S): A new tool to evaluate plate locking along subduction zones. Journal of Geophysical Research, Solid Earth 121 (2): 469-490. https://doi.org/10.1002/2015JB012382

Hervé, M. 1976. Estudio geológico de la falla Liquiñe-Reloncaví en el área de Liquiñe-Reloncaví, antecedentes de un movimiento transcurrente (Provincia de Valdivia). *In* Congreso Geológico Chileno, No. 1, Actas 1: B39-B56. Santiago.

Hervé, F. 1994. The Southern Andes between 39° and 44° S Latitude: The Geological Signature of a Transpressive Tectonic Regime Related to a Magmatic Arc. *In* Tectonics of the Southern Central Andes Reutter (Reutter, K.J.; Scheuber, E.; Wigger, P.J.; editors). Springer Verlag: 243-248. Berlin. https://doi.org/10.1007/978-3-642-77353-2_17

Hervé, F.; Araya, E.; Fuenzalida, J.L.; Solano, A. 1979. Edades radiométricas y tectónica neógena en el sector costero de Chiloé Continental, X Región. *In* Congreso Geológico Chileno, No. 2, Actas 1: FI-F8. Arica.

Hervé, F.; Pankhurst, R.J.; Drake, R.; Beck, M.E. 1995. Pillow metabasalts in a mid-Tertiary extensional basin adjacent to the Liquiñe-Ofqui fault zone: the Isla Magdalena area, Aysén, Chile. Journal of South American Earth Sciences 8 (1): 33-46. https://doi.org/10.1016/0895-9811(94)00039-5

Iturrieta, P.C.; Hurtado, D.E.; Cembrano, J.; Stanton-Yonge, A. 2017. States of stress and slip partitioning in a continental-scale strike-slip duplex: Tectonic and magmatic implications by means of finite element modeling. Earth and Planetary Science Letters 473 (1): 71-82. https://doi.org/10.1016/j.epsl.2017.05.041

Jarrard, R.D. 1986. Relations among subduction parameters. Reviews of Geophysics 24 (2): 217-284. https://doi.org/10.1029/RG024i002p00217

Johnson, S.Y.; Blakely, R.J.; Stephenson, W.J.; Dadisman, S.V.; Fisher, M.A. 2004. Active shortening of the Cascadia forearc and implications for seismic hazards of the Puget Lowland. Tectonics 23 (1): 1-27. https://doi.org/10.1029/2003TC001507

Jordan, T.E.; Isacks, B.L.; Allmendinger, R.W.; Brewer, J.A.; Ramos, V.A.; Ando, C.J. 1983. Andean tectonics related to geometry of subducted Nazca plate. Geological Society of America Bulletin 94 (3): 341-361. https://doi.org/10.1130/0016-7606(1983)94%3C341:ATRTGO%3E2.0.CO;2

Kirkpatrick, J.D.; Rowe, C.D. 2013. Disappearing ink: How pseudotachylytes are lost from the rock record. Journal of Structural Geology 52: 183-198. https://doi.org/10.1016/j.jsg.2013.03.003

Lange, D.; Cembrano, J.; Rietbrock, A.; Haberland, C.; Dahm, T.; Bataille, K. 2008. First seismic record for intra-arc strike-slip tectonics along the Liquiñe-Ofqui fault zone at the obliquely convergent plate margin of the southern Andes. Tectonophysics 445 (1-4): 14-24. https://doi.org/10.1016/j.tecto.2008.04.014

Lara, L.E.; Naranjo, J.A.; Moreno, H. 2004. Rhyodacitic fissure eruption in the Southern Andes (Cordón Caulle; 40.5° S) after the 1960 (Mw 9.5) Chilean earthquake: A structural interpretation. Journal of Volcanology and Geothermal Research 138 (1-2): 127-138. https://doi.org/10.1016/j.jvolgeores.2004.06.009

Lara, L.; Lavenu, A.; Cembrano, J.; Rodríguez, C. 2006. Structural controls of volcanism in transversal chains: Resheared faults and neotectonics in the Cordón Caulle-Puyehue area (40.5ºS), Southern Andes. Journal of Volcanology and Geothermal Research 158 (1-2): 70-86. https://doi.org/10.1016/j.jvolgeores.2006.04.017

Lavenu, A.; Cembrano, J. 1999. Compressional- and transpressional-stress pattern for Pliocene and Quaternary brittle deformation in fore arc and intra-arc zones (Andes of Central and Southern Chile). Journal of Structural Geology 21 (12): 1669-1691. https://doi.org/10.1016/S0191-8141(99)00111-X

Lavenu, A.; Cembrano, J. 2008. Quaternary compressional deformation in the Main Cordillera of Central Chile (Cajón del Maipo, east of Santiago). Revista Geológica de Chile 35 (2): 233-252. http://dx.doi.org/10.5027/andgeoV35n2-a03

Lavenu, A.; Thiele, R.; Machette, M.; Dart, R.; Bradley, L.-A.; Haller, K.M. 2000. Maps and database of Quaternary faults in Bolivia and Chile. United States Geological Survey, Open-File Report 00-283: 46 p.

Legrand, D.; Barrientos, S.; Bataille, K.; Cembrano, J.; Pavez, A. 2011. The fluid-driven tectonic swarm of Aysen Fjord, Chile (2007) associated with two earthquakes (Mw=6.1 and Mw=6.2) within the Liquiñe-Ofqui Fault Zone. Continental Shelf Research 31 (3-4): 154-161. https://doi.org/10.1016/j.csr.2010.05.008

Lockner, D.A. 1995. Rock failure. Rock physics and phase relations: A handbook of physical constants (3):127-147.

Maldonado, V.; Contreras, M.; Melnick, D. 2021. A comprehensive database of active and potentially-active continental faults in Chile at 1:25,000 scale. Scientific Data 8 (20). https://doi.org/10.1038/s41597-021-00802-4

Marrett, R.; Allmendinger, R.W. 1990. Kinematic analysis of fault-slip data. Journal of Structural Geology 12 (8): 973-986. https://doi.org/10.1016/0191-8141(90)90093-E

McCaffrey, R. 1992. Oblique plate convergence, slip vectors, and forearc deformation. Journal of Geophysical Research, Solid Earth 97 (B6): 8905-8915. https://doi.org/10.1029/92JB00483

McCaffrey, R. 1996. Slip partitioning at convergent plate boundaries of SE Asia. Geological Society, London, Special Publications 106: 3-18. https://doi.org/10.1144/GSL.SP.1996.106.01.02

Mc Kinnon, S.; Garrido de la Barra, I. 2003. Stress field analysis at the El Teniente Mine: Evidence for N-S compression in the modern Andes. Journal of Structural Geology 25 (12): 2125-2139.

Melnick, D.; Charlet, F.; Echtler, H.P., De Batist, M. 2006. Incipient axial collapse of the Main Cordillera and strain partitioning gradient between the central and Patagonian Andes, Lago Laja, Chile. Tectonics 25 (5): 1-22. https://doi.org/10.1029/2005TC001918

Melnick, D.; Bookhagen, B.; Strecker, M.R.; Echtler, H.P. 2009. Segmentation of megathrust rupture zones from fore-arc deformation patterns over hundreds to millions of years, Arauco peninsula, Chile. Journal of Geophysical Research 114 (B1): B01407. https://doi.org/10.1029/2008JB005788

Mescua, J.F.; Barrionuevo, M.; Giambiagi, L.; Suriano, J.; Spagnotto, S.; Stahlschmidt, E.; De la Cal, H.; Soto, J.L.; Mazzitelli, M.A. 2019. Stress field and active faults in the orogenic front of the Andes in the Malargüe fold-and-thrust belt (35º-36ºS). Tectonophysics 766: 179-193. https://doi.org/10.1016/j.tecto.2019.06.003

Montenegro, V.M.; Spagnotto, S.; Legrand, D.; Caselli, A.T. 2021. Seismic evidence of the active regional tectonic faults and the Copahue volcano, at Caviahue Caldera, Argentina. Bulletin of Volcanology 83 (20). https://doi.org/10.1007/s00445-021-01442-7

Mora, C.; Comte, D.; Russo, R.; Gallego, A.; Mocanu, V. 2010. Aysén seismic swarm (January 2007) in southern Chile: analysis using Joint Hypocenter Determination. Journal of Seismology 14: 683-691. https://doi.org/10.1007/s10950-010-9190-y

Moreno, M.S.; Bolte, J.; Klotz, J.; Melnick, D. 2009. Impact of megathrust geometry on inversion of coseismic slip from geodetic data: Application to the 1960 Chile earthquake. Geophysical Research Letters 36 (16). https://doi.org/10.1029/2009GL039276

Moreno, M.; Melnick, D.; Rosenau, M.; Baez, J.; Klotz, J.; Oncken, O.; Tassara, A.; Chen, J.; Bataille, K.; Bevis, M.; Socquet, A.; Bolte, J.; Vigny, C.; Brooks, B.; Ryder, I.; Grund, V.; Smalley, B.; Carrizo, D.; Bartsch, M.; Hase. H. 2012. Toward understanding tectonic control on the Mw 8.8 2010 Maule Chile earthquake. Earth and Planetary Science Letters 321-322: 152-165. https://doi.org/10.1016/j.epsl.2012.01.006

Moreno, M.; Bedford, J.R.; Schurr, B.; Báez, J.C.; Urrutia, I.; Lange, D.; Oncken, O.; Melnick, D. 2016. From locking to coupling: Investigating the links between kinematics and stress accumulation along the Chilean subduction Zone. In AGU Fall Meeting, Abstract G32A-01. San Francisco.

Mura, V.; Arancibia, G.; Browning, J.; Healy, D.; López-Contreras, C.; Morata, D.; Maza, S.; Cardona, C. 2025. Structural control on the Southern Andean Nevados de Chillán geothermal system. Journal of Structural Geology 196. https://doi.org/10.1016/j.jsg.2025.105380

Niemeijer, A.; Di Toro, G.; Nielsen, S.; Di Felice, F. 2011. Frictional melting of gabbro under extreme experimental conditions of normal stress, acceleration, and sliding velocity. Journal of Geophysical Research, Solid Earth 116 (B7): 1-18. https://doi.org/10.1029/2010JB008181

Noda, H.; Lapusta, N. 2013. Stable creeping fault segments can become destructive as a result of dynamic weakening. Nature 493: 518-521. https://doi.org/10.1038/nature11703

Olivar, J.; Nacif, S.; García, H.; Fennell, L.; Heit, B.; Folguera, A. 2022. Controls on crustal seismicity segmentation on a local scale in the Southern Central Andes. Journal of South American Earth Sciences 116. https://doi.org/10.1016/j.jsames.2022.103778

Pardo-Casas, F.; Molnar, P. 1987. Relative motion of the Nazca (Farallon) and South American plates since late Cretaceous time. Tectonics 6 (3): 233-248. https://doi.org/10.1029/TC006i003p00233

Pearce, R.K.; Sánchez de la Muela, A.; Moorkamp, M.; Hammond, J.O.S.; Mitchell, T.M.; Cembrano, J.; Araya Vargas, J.; Meredith, P.G.; Iturrieta, P.; Pérez-Estay, N.; Marshall, N.R.; Smith, J.; Yañez, G.; Griffith, W.A.; Marquardt, C.; Stanton-Yonge, A.; Núñez, R. 2020. Reactivation of fault systems by compartmentalized hydrothermal fluids in the Southern Andes revealed by magnetotelluric and seismic data. Tectonics 39 (12). https://doi.org/10.1029/2019TC005997

Pérez-Estay, N.; Yáñez, G.; Crempien, J.; Roquer, T.; Cembrano, J.; Valdenegro, P.; Aravena, D.; Arancibia, G.; Morata, D. 2020. Seismicity in a transpressional volcanic arc: The Liquiñe-Ofqui Fault System in the Puyuhuapi Area, Southern Andes, Chile (44º S). Tectonics 39 (11). https://doi.org/10.1029/2020TC006391

Pérez-Estay, M.; Ruz-Ginouves, J.; Pérez-Flores, P.; Sielfeld, G.; Roquer, T.; Cembrano, J. 2023. Decoding the state of stress and fluid pathways along the Andean Southern Volcanic Zone. Communications Earth & Environment 4: 390. https://doi.org/10.1038/s43247-023-01040-9

Pérez-Flores, P.; Cembrano, J.; Sánchez-Alfaro, P.; Veloso, E.; Arancibia, G.; Roquer, T. 2016. Tectonics, magmatism and paleo-fluid distribution in a strike-slip setting: Insights from the northern termination of the Liquiñe-Ofqui fault System, Chile. Tectonophysics 680: 192-210. https://doi.org/10.1016/j.tecto.2016.05.016

Petit, J.P. 1987. Criteria for the sense of movement on fault surfaces in brittle rocks. Journal of Structural Geology 9 (5-6): 597-608. https://doi.org/10.1016/0191-8141(87)90145-3

Piquer, J.; Castelli, J.C.; Charrier, R.; Yáñez, G. 2010. The Cenozoic of the upper Teno River, Cordillera Principal, Central Chile: stratigraphy, plutonism and their relation with deep structures. Andean Geology 37 (1): 32-53. http://dx.doi.org/10.5027/andgeoV37n1-a2

Piquer, J.; Skarmeta, J.; Cooke, D.R. 2015. Structural evolution of the Rio Blanco-Los Bronces District, Andes of Central Chile: controls on stratigraphy, magmatism, and mineralization. Economic Geology 110 (8): 1995-2023. https://doi.org/10.2113/econgeo.110.8.1995

Piquer, J.; Rivera, O.; Yáñez, G.; Oyarzún, N. 2021. The Piuquencillo fault system: a long-lived, Andean-transverse fault system and its relationship with magmatic and hydrothermal activity. Solid Earth 12 (1): 253-273. https://doi.org/10.5194/se-12-253-2021

Potin, B.; Ruiz, S.; Aden-Antoniow, F.; Madariaga, R.; Barrientos, S. 2025. A revised Chilean seismic catalog from 1982 to mid-2020. Seismological Research Letters 96 (1): 484-498. https://doi.org/10.1785/0220240047

Quiero, F.; Tassara, A.; Iaffaldano, G.; Rabbia, O. 2022. Growth of Neogene Andes linked to changes in plate convergence using high-resolution kinematic models. Nature Communications 13. https://doi.org/10.1038/s41467-022-29055-4

Ramos, V.A.; Jordan, T.E.; Allmendinger, R.W.; Mpodozis, C.; Kay, S. M. ; Cortés, J.M. ; Palma, M. 1986. Paleozoic terranes of the central Argentine-Chilean Andes. Tectonics, 5 (6): 855-880. https://doi.org/10.1029/TC005i006p00855

Rivera, O.; Cembrano, J. 2000. Modelo de formación de cuencas volcano-tectónicas en zonas de transferencia oblicuas a la cadena andina: El caso de las cuencas oligo-miocénicas de Chile central y su relación con estructuras NWW-NW (33º00'-34º30' S). *In* Congreso Geológico Chileno, No. 9, Actas 1: 631-636. Puerto Varas.

Rojas, C.; Beck, M.E. Jr.; Burmester, R.F.; Cembrano, J.; Hervé, F. 1994. Paleomagnetism of the Mid-Tertiary Ayacara Formation, southern Chile: counterclockwise rotation in a dextral shear zone. Journal of South American Earth Sciences 7 (1): 45-56. https://doi.org/10.1016/0895-9811(94)90033-7

Roquer, T.; Arancibia, G.; Crempien, J.G.; Mery, D.; Rowland, J.; Sepúlveda, J.; Veloso, E.E.: Nehler, M.;

Bracke, R.; Morata, D. 2022. Multi-scale flow structure of a strike-slip tectonic setting: A self-similar model for the Liquiñe-Ofqui Fault System and the Andean Transverse Faults, Southern Andes (39-40°S). Geothermics 103. https://doi.org/10.1016/j.geothermics.2022.102424

Rosenau, M.; Melnick, D.; Echtler, H. 2006. Kinematic constraints on intra-arc shear and strain partitioning in the southern Andes between 38º S and 42º S latitude. Tectonics 25 (4): 1-16. https://doi.org/10.1029/2005TC001943

Rousset, B. 2019. Months-long subduction slow slip events avoid the stress shadows of seismic asperities. Journal of Geophysical Research: Solid Earth 124 (7): 7337-7230. https://doi.org/10.1029/2019JB018037

Rowe, C.D.; Griffith, W.A. 2015. Do faults preserve a record of seismic slip? A second opinion. Journal of Structural Geology 78: 1-26. https://doi.org/10.1016/j.jsg.2015.06.006

Rowland, J.V.; Simmons, S.F. 2012. Hydrologic, magmatic, and tectonic controls on hydrothermal flow, Taupo Volcanic Zone, New Zealand: Implications for the formation of epithermal vein deposits. Economic Geology 107 (3): 427-457. https://doi.org/10.2113/econgeo.107.3.427

Rutter, E.H. 1983. Pressure solution in nature, theory and experiment. Journal of the Geological Society 140 (5): 725-740. https://doi.org/10.1144/gsjgs.140.5.0725

Ruz-Ginouves, J.; Browning, J.; Cembrano, J.; Iturrieta, P.; Gerbault, M.; Sielfeld, G. 2020. Field observations and numerical models of a Pleistocene-Holocene feeder dyke swarm associated with a fissure complex to the east of the Tatara-San Pedro-Pellado complex, Southern Volcanic Zone, Chile. Journal of Volcanology and Geothermal Research 404. https://doi.org/10.1016/j.jvolgeores.2020.107033

Sánchez, P.; Pérez-Flores, P.; Arancibia, G.; Cembrano, J.; Reich, M. 2013. Crustal deformation effects on the chemical evolution of geothermal systems: the intra-arc Liquiñe-Ofqui fault system, Southern Andes. International Geology Review 55 (11): 1384-1400. https://doi.org/10.1080/00206814.2013.775731

Santibáñez, I.; Cembrano, J.; García-Pérez, T.; Costa, C.; Yáñez, G.; Marquardt, C.; Arancibia, G.; González, G. 2019. Crustal faults in the Chilean Andes: geological constraints and seismic potential. Andean Geology 46 (1): 32-68. http://dx.doi.org/10.5027/andgeoV46n1-3067

Savran, W. H.; Bayona, J. A.; Iturrieta, P.; Asim, K. M.; Bao, H.; Bayliss, K.; Herrmann, M.; Schorlemmer, D.; Marchling, P.J.; Werner, M.J. 2022. pyCSEP: A Python toolkit for earthquake forecast developers. Seismological Research Letters 93 (5): 2858-2870. https://doi.org/10.1785/0220220033

Seebeck, H.; Van Dissen, R.; Litchfield, N.; Barnes, P.M.; Nicol, A. Langridge, R.; Barrell, D.J.A.; Villamor, P.; Ellis, S.; Rattenbury, M.; Bannister, S.; Gerstenberger, M.; Ghisetti, F.; Sutherland, R.; Hirschberg, H.; Fraser, J.; Nodder, S.D.; Stirling, M.; Humphrey, J.; Bland, K.J.; Howell, A.; Mountjoy, J.; Moon, V.; Stahl, T.; Spinardi, F.; Townsend, D.; Clark, K.; Hamling, I.; Cox, S.; de Lange, W.; Wopereis, P.; Johnston, M.; Morgenstern, R.; Coffey, G.; Eccles, J.D.; Little, T.; Fry, B.; Griffin, J.; Townend, J.; Mortimer, N.; Alcaraz, S.; Massiot, C.; Rowland, J.V.; Muirhead, J.; Upton, P.; Lee, J. 2023. The New Zealand Community Fault Model-version 1.0: An improved geological foundation for seismic hazard modelling. New Zealand Journal of Geology and Geophysics 67 (2): 209-229. https://doi.org/10.1080/00288306.2023.2181362

Sernageomin. 2003. Mapa Geológico de Chile: versión digital. Servicio Nacional de Geología y Minería, Publicación Geológica Digital No. 4 (CD-ROM, versión 1.0, 2003). Santiago.

Sielfeld, G.; Cembrano, J.; Lara, L. 2017. Transtension driving volcano-edifice anatomy: Insights from Andean transverse-to-the-orogen tectonic domains. Quaternary International 438: 33-49. https://doi.org/10.1016/j.quaint.2016.01.002

Sielfeld, G.; Lange, D.; Cembrano, J. 2019a. Intra-arc crustal seismicity: Seismotectonic implications for the Southern Andes Volcanic Zone, Chile. Tectonics 38: 552-578. https://doi.org/10.1029/2018TC004985

Sielfeld, G.; Ruz, J.; Brogi, A.; Cembrano, J.; Stanton-Yonge, A.; Pérez-Flores, P.; Iturrieta, P. 2019b. Oblique-slip tectonics in an active volcanic chain: A case study from the Southern Andes. Tectonophysics 770. https://doi.org/10.1016/j.tecto.2019.228221

Somoza, R. 1998. Updated Nazca (Farallon)-South America relative motions during the last 40 My: implications for mountain building in the central Andean region. Journal of South American Sciences 11 (3): 211-215. https://doi.org/10.1016/S0895-9811(98)00012-1

Stanton-Yonge, A.; Griffith, W.A.; Cembrano, J.; St. Julien, R.; Iturrieta, P. 2016. Tectonic role of margin-parallel and margin-transverse faults during oblique subduction in the Southern Volcanic Zone of the Andes: Insights from Boundary Element Modeling. Tectonics 35 (9): 1990-2013. https://doi.org/10.1002/2016TC004226

Stanton-Yonge, A.; Sánchez de la Muela, A.; Pearce, R.K.; Hammond, J.O.S.; Mitchell, T.M.; Hicks, S.P.; Griffith, W.A. ; Moorkamp, M.; Meredith, P.; Cembrano, J. 2025. Fluid pressure fluctuations and the seismic signature of a fault-controlled fluid migration pulse. Earth and Planetary Science Letters 662. https://doi.org/10.1016/j.epsl.2025.119388

Stern, C.R.; Skewes, M.A.; Arévalo, A. 2011. Magmatic evolution of the giant El Teniente Cu-Mo Deposit, Central Chile. Journal of Petrology 52 (7-8): 1591-1617. https://doi.org/10.1093/petrology/egq029

Tapia, F.; Farías, M.; Naipauer, M.; Puratich, J. 2015. Late Cenozoic contractional evolution of the current arc-volcanic region along the southern Central Andes (35°20' S). Journal of Geodynamics 88: 36-51. https://doi.org/10.1016/j.jog.2015.01.001

Tassara, A.; Yáñez, G. 2003. Relación entre el espesor elástico de la litósfera y la segmentación tectónica del margen andino (15-47º S). Andean Geology 30 (2): 159-186. http://dx.doi.org/10.4067/S0716-02082003000200002

Teyssier, C.; Tikoff, B.; Markley, M. 1995. Oblique plate motion and continental tectonics. Geology 23 (5): 447-450. https://doi.org/10.1130/0091-7613(1995)023%3C0447:OPMACT%3E2.3.CO;2

Thompson, S.N. 2002. Late Cenozoic geomorphic and tectonic evolution of the Patagonian Andes between latitudes 42º S and 46º S: An appraisal based on fission-track results from the transpressional intra-arc Liquiñe-Ofqui fault zone. Geological Society of America Bulletin 114 (9): 1159-1173. https://doi.org/10.1130/0016-7606(2002)114%3C1159:LCGATE%3E2.0.CO;2

USGS. 2017. Advanced National Seismic System (ANSS) Comprehensive Earthquake Catalog. United States Geological Survey. https://earthquake.usgs.gov/data/comcat/

Vargas, G.; Klinger, Y.; Rockwell, T.K.; Forman, S.L.; Rebolledo, S.; Baize, S.; Lacassin, R.; Armijo, R. 2014. Probing large intraplate earthquakes at the west flank of the Andes. Geology 42 (12): 1083-1086. https://doi.org/10.1130/G35741.1

Vega-Ruiz, A.; Cortés-Aranda, J.; Aguilera-Cortés, R.; Astudillo-Sotomayor, L.; Riedel, M.; Espinoza, M.; Tassara, A.; Nelson, A.; Melnick, D.; Lupi, M.; Arriagada, D.; Sepúlveda, T.; Álvarez-Amado, F.; Navarro, L. 2025. Pliocene to Holocene deformation and earthquake potential of the Mesamávida Fault, West Andean Thrust System of Central-Southern Chile (36° S). Tectonics 44 (7). https://doi.org/10.31223/X5T153

Vigide, N.; Olivar, J.; Mescua, J.; Basualto, D.; Farías, C.; Tassara, A.; García, S. 2025. A transpressive stress regime for the Laguna del Maule Volcanic Complex. Journal of South American Earth Sciences 161. https://doi.org/10.1016/j.jsames.2025.105563

Vigny, C.; Socquet, A.; Peyrat, S.; Ruegg, J.C.; Métois, M.; Madariaga, R.; Morvan, S.; Lancieri, M.; Lacassin, R.; Campos, J.; Carrizo, D.; Bejar-Pizarro, M.; Barrientos, S.; Armijo, R.; Aranda, C.; Valderas-Bermejo, M.-C.; Ortega, I.; Bondoux, F.; Baize, S.; Lyon-Caen, H.; Pavez, A.; Vilotte, J.P.; Bevis, M.; Brooks, B.; Smalley, R.; Parra, H.; Báez, J.-C.; Blanco, M.; Cimbaro, S.; Kendrick, E. 2011.The 2010 Mw 8.8 Maule Megathrust earthquake of Central Chile, monitored by GPS. Science 332 (6036): 1417-1421. https://doi.org/10.1126/science.1204132

Wall, R.; Gana, P.; Gutiérrez, A. 1996. Mapa geológico del área de San Antonio-Melipilla, regiones de Valparaíso, Metropolitana y del Libertador General Bernardo O'Higgins. Servicio Nacional de Geología y Minería, Mapas Geológicos 2, 1 mapa escala 1:100.000, 1 anexo. Santiago.

Wang, K.; Hu, Y.; Bevis, M.; Kendrick, E.; Smalley, R. Jr.; Barriga Vargas, R.; Lauría, E. 2007. Crustal motion in the zone of the 1960 Chile earthquake: Detangling earthquake-cycle deformation and forearc-sliver translation. Geochemistry, Geophysics, Geosystems 8 (10): 1-14. https://doi.org/10.1029/2007GC001721

Weatherill, G. A.; Pagani, M.; Garcia, J. 2016. Exploring earthquake databases for the creation of magnitude-homogeneous catalogues: tools for application on a regional and global scale. Geophysical Journal International 206 (3): 1652-1676. https://doi.org/10.1093/gji/ggw232

Weller, O.; Lange, D.; Tilmann, F.; Natawidjaja, D.; Rietbrock, A.; Collings, R.; Gregory, L. 2012. The structure of the Sumatran Fault revealed by local seismicity. Geophysical Research Letters 39 (1): 1-7. https://doi.org/10.1029/2011GL050440

Yáñez, G.A.; Gana, P.; Fernández, R. 1998. Origen y significado geológico de la Anomalía Melipilla, Chile central. Revista Geológica de Chile 25 (2): 175-198. http://dx.doi.org/10.4067/S0716-02081998000200005

Yáñez, G.; Pérez-Estay, N.; Araya-Vargas, J.; Sanhueza, J.; Figueroa, R.; Maringue, J.; Rojas, T. 2020. Shallow anatomy of the San Ramón Fault (Chile) constrained by geophysical methods: Implications for its role in the Andean deformation. Tectonics 39 (8): 1-21. https://doi.org/10.1029/2020TC006294

Yáñez, G.; Piquer, J.; Rivera, O. 2024. On the role of trans-lithospheric faults in the long-term seismotectonic segmentation of active margins: a case study in the Andes. European Geosciences Union 15 (11): 1319-1342. https://doi.org/10.5194/se-15-1319-2024

Youngs, R.; Coppersmith, K. 1985. Implications of fault slip rates and earthquake recurrence models to probabilistic seismic hazard estimates. Bulletin of the Seismological Society of America 75 (4): 939-964. https://doi.org/10.1016/0148-9062(86)90651-0

Manuscript received: October 14, 2025; revised/accepted: April 28, 2026; available online: April 29, 2026.